Investigation of an extreme rainfall event during 8–12 December 2018 over central Viet Nam – Part 2: An evaluation of predictability using a time-lagged cloud-resolving ensemble system

Chung-Chieh Wang[1], Duc Van Nguyen[1,2], Thang Van Vu[2], Pham Thi Thanh Nga[2], Pi-Yu Chuang[1], and Kien Ba Truong[2,*]

Correspondence: kien.cbg@gmail.com

[1]Department of Earth Sciences, National Taiwan Normal University, Taipei, Taiwan

[2]Viet Nam Institute of Meteorology, Hydrology and Climate Change, Hanoi, Viet Nam

Abstract:

This is the second part of a two-part study that investigates an extreme rainfall event that occurred from 8 to 12 December 2018 over central Viet Nam (referred to as the D18 event). In this part, the study aims to evaluate the practical predictability of the D18 event using the quantitative precipitation forecasts (QPFs) from a time-lagged cloud-resolving ensemble system. To do this, 29 time-lagged (8 days in forecast range) high resolution (2.5 km) members were run, with the first member initialized at 12:00 UTC 3 December and the last one at 12:00 UTC 10 December 2018. Between the first and the last members are multiple members that were executed every 6 h. The evaluation results reveal that the cloud-resolving model (CReSS) well predicted the rainfall fields at the short range (less than 3 days) for 10 December (the rainiest day). Particularly, the CReSS shows high skill in heavy-rainfall QPFs for this date with a Similarity Skill Score (SSS) greater than 0.5 for both the last five members and the last nine members. The good results are due to the model having good predictions of relevant meteorological variables such as surface winds. However, the predictive skill is reduced at lead times longer than 3 days, and it is challenging to achieve good QPFs for rainfall thresholds greater than 100 mm at lead times longer than 6 days. These results also confirmed our scientific hypothesis that the cloud-resolving time-lagged ensemble system (using the CReSS model) improved the QPFs of

27 this event at the short range. Furthermore, the results also demonstrated that a decent QPF

28 can be made at a longer lead time (by a member initialized at 1800 UTC 4 December).

29 In addition, the ensemble-based sensitivity analysis (ESA) of 24-h rainfall in central Viet

30 Nam shows that it is highly sensitive to initial conditions, not only at lower levels but also

31 at upper levels. The rainfall is sensitive to both kinematics and moisture convergence at

32 low levels, and such sensitivities decrease with increasing lead time. The ESA also

33 facilitates a better understanding of the mechanisms in the D18 event, implying that it is

34 meaningful to apply ESA to control initial conditions in the future.

1 Introduction

36 The present study is the second part of a two-part study investigating the extreme rainfall

37 event during 8–12 December 2018 over central Viet Nam (referred to as the D18 event

38 hereafter). In this event, record-breaking rainfall occurred along the mid-central coast of

39 Viet Nam, from Quang Binh to Quang Ngai provinces. The observation shows that the

40 peak amount in rainfall accumulation, in particular, exceeded 800 mm over a 3-day period

41 from 12:00 UTC 8 to 12:00 UTC 11 December (Fig. 1f). During this period, the rainiest

42 day was 10 December with 24-h observed amount exceeding 600 mm at some stations (Fig.

43 4 OBS). This record-breaking rainfall event led to 13 deaths, widespread destructions in

44 the environment and downstream cities, and heavy economic losses due to catastrophic

45 flooding and landslides (Tuoi Tre news, 2018). In part 1 (Wang and Nguyen 2023), we

46 focused on the analysis of the mechanism that caused this event and evaluated the

47 simulation by the Cloud-Resolving Storm Simulator (CReSS; Tsuboki and Sakakibara,

48 2002, 2007). The analysis results point out the main factors which led to this event as well

49 as its spatial rainfall distribution. These factors included the combined interaction between

50 the strong northeasterly winds and easterly winds over the South China Sea (SCS) in the

51 lower troposphere (below 700 hPa). The local terrain also played essential role due to its

52 barrier effect. The cloud model's good simulation results in part 1 indicated its promising

53 potential in forecasting this event. Hence, in part 2, the present study focuses on an

54 evaluation of its predictability of the D18 event through a series of time-lagged high-

55 resolution ensemble quantitative precipitation forecasts (QPFs) by the CReSS model.

56 Predicting heavy rainfall events is still challenging to meteorologists and weather

57 forecasters, although great progresses have been made in the science of numerical weather

58 prediction. The prediction of heavy to extreme rainfall is more difficult for Viet Nam,

59 where both multi-scale interactions among different weather systems and strong influence

60 by local topography often exist. For example, when D18 event occurred, several

61 operational models were unable to predict this event successfully. Specifically, Fig. 1

62 shows the predictions for the D18 event by three global models at the National Centers for

63 Environmental Prediction (NCEP), the European Centre for Medium-Range Weather

64 Forecasts (ECMWF), and the Japan Meteorological Agency (JMA), and by one mesoscale

65 regional model, the Weather Research and Forecasting (WRF) model, implemented for

66 operation at the Mid-central regional Hydro-Meteorological center in Da Nang city, Viet

67 Nam, with the finest horizontal grid spacing (Δx) of 6 km × 6 km. While these models

68 overall made good predictions in the surface wind field, their 72-h accumulated rainfall

69 amounts along the coast of central Viet Nam were less than 250 mm and much lower than

70 the observation, which exceeded 900 mm (Fig. 1). Therefore, in order to improve the QPFs

71 for heavy rainfall events in Viet Nam, we need to not only understand their mechanisms of

72 occurrence, but also adopt or develop better forecasting tools, more effective strategy, or

73 both.
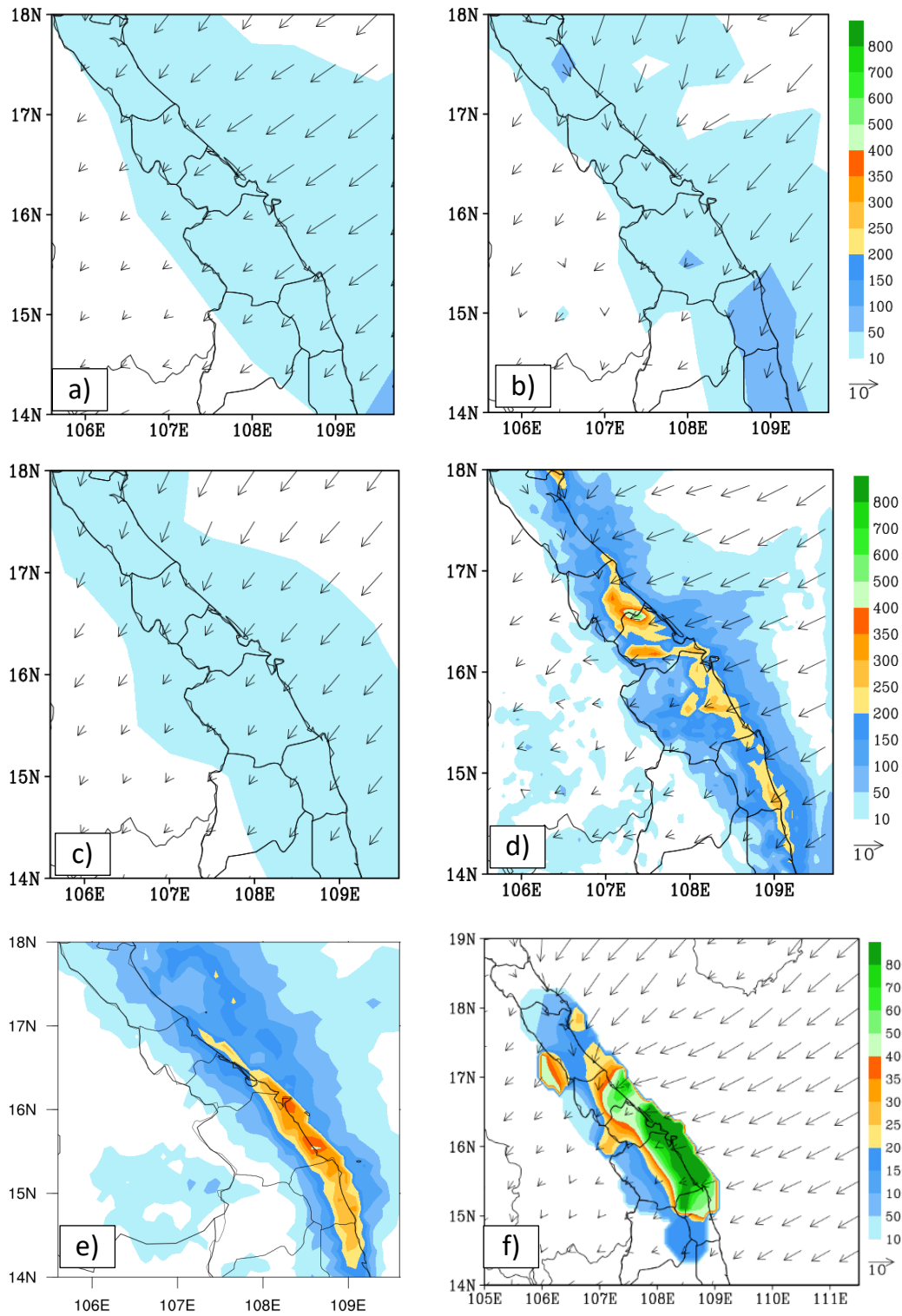
Figure 1. The predicted 72h accumulated rainfall (mm, shaded) and mean surface wind
(ms⁻¹, vector) for the period of 12:00 UTC 8 December – 12:00 UTC 11 December 2018
obtained by (a) NCEP, (b) ECMWF, (c) JMA, (d) WRF, (e) 72h accumulated rainfall
obtained by the Global Precipitation Measurement (GPM) estimate (IMERG Final Run

product) and (f) 72h in-situ observed accumulated rainfall (mm, shaded) and the mean surface wind derived from ERA5 data (ms^{-1}, vector), adapted from Fig. 14c of Wang and Nguyen (2023).

Among several different methods, present-day weather forecasts depend mainly on numerical weather prediction (NWP) using models, a scientific method that has become indispensable for its ability to simulate weather and produce quantitative results (Fig. 1). However, there is always uncertainty in numerical forecasts due to the fact that the atmosphere is a chaotic system and tiny errors in the initial state can grow rapidly and lead to larger errors in the forecast (Hohenegger and Schär, 2007, Lorenz 1969). Various approximations in numerical methods are also sources of forecast uncertainty. Thus, by generating a range of possible weather conditions in days ahead or into the future, the ensemble forecasting was introduced as an effective method to estimate forecast uncertainty and improve the overall accuracy and usefulness of NWP products. This is because the ensemble mean typically has smaller errors than individual members, since the high predictability features that the members agree on are emphasized by the mean, while the low-predictability ones that the members do not agree on are filtered out or dampened (e.g., Leith 1974; Murphy 1988, Surcel et al. 2014). Furthermore, some studies have shown high skill in QPFs for extreme rainfall produced by typhoons in Taiwan using the CReSS model, a cloud-resolving model (CRM), with high resolution and time-lagged approach (Wang et al. 2016; Wang 2015; Wang et al. 2014; Wang et al. 2013). Table 1 of Wang et al. (2016) shows that the high-resolution time-lagged ensemble forecasts provide overall better quality in comparison with both the traditional low-resolution ensemble forecasts and high-resolution deterministic forecasts at a comparable cost in computation.

Besides the advantages of ensemble forecasts described above, the ensemble-based sensitivity analysis (ESA) also provides an effective method to investigate how sensitive the forecast variables are and to what preceding factors. To be more specific, Torn and Hakim (2009) used ESA to evaluate how their subject, a group of tropical cyclones (TCs) undergoing extratropical transition, in the prediction respond to changes in the initial

108   condition. In their results, the cyclone minimum sea-level pressure forecasts are determined

109   as strongly sensitive to TC intensity and position at short lead times and equally sensitive

110   to mid-latitude troughs that interacted with the TC at longer lead times. For an extreme

111   rainfall event in northern Taiwan, Wang et al. (2021) performed ESA using the results from

112   45 forecast members with grid sizes of 2.5–5 km to identify contributing factors to heavy

113   rainfall. By normalizing their impacts on rainfall using standard deviation (SD), different

114   factors can be compared quantitatively and on an equal footing. Ranked by their

115   importance, these factors included the position of the surface Mei-yu front and its moving

116   speed, the position of 700-hPa wind shift line and its speed, the moisture amount in the

117   environment near the front, timing and location of frontal mesoscale low-pressure

118   disturbance, and frontal intensity. Many other studies also used the ESA to study TCs,

119   convective events, or support the development of operational ensemble sensitivity-based

120   techniques to improve probabilistic forecasts (e.g., Kerr et al. 2019, Hu and Wu 2020,

121   Coleman and Ancell 2020).

122   While ensemble-based sensitivity analysis provides valuable insights into key drivers of

123   forecast outcomes as reviewed above, its effectiveness is inherently tied to the limits of

124   predictability. Generally, the atmospheric predictability can be categorized into two types:

125   practical predictability and intrinsic predictability (Melhauser and Zhang 2012, Nielsen

126   and Schumacher 2016, Ying and Zhang 2017, Weyn and Durran 2018). Intrinsic

127   predictability represents the highest achievable predictability using a nearly perfect initial

128   conditions and a nearly perfect forecast model, and is mainly depended on scale and types

129   of weather systems. Whereas, practical predictability describes the predictability using the

130   best-available techniques and initial conditions, and therefore it can be limited by

131   uncertainties in both the model and initial conditions. According to the studies cited above,

132   practical predictability can be improved by improving the initial conditions, but it however

133   cannot exceed the intrinsic predictability (Ying and Zhang 2017). Based on these, in our

134   study, we investigate the practical predictability of the D18 event because it is a real event.

For heavy precipitation over central Viet Nam, Son and Tan (2009) used the Mesoscale Model version 5 (MM5) to investigate the predictability of heavy-rainfall events over the southern part of central Viet Nam during the period of 2005 and 2007. In this study, experiments were configured for two nested domains with Δx of 27 and 9 km, respectively. Their results showed that the MM5 can predict heavy rainfall there and its performance is better for events caused by TCs or TC interactions with the cold air. Toan et al. (2018) assessed the predictability of heavy rainfall events in middle-central Viet Nam due to combined effects of cold air and easterly winds using the WRF model within a forecast range of 2 days. The model was also set with two nesting domains. The outer domain (D1) covers the entire Vietnam and SCS with a Δx of 18 km, while the inner domain (D2) focuses on the Mid-Central Vietnam region with a Δx of 6 km. The evaluation indicated that at 24-h lead time, the model performed reasonably well at rainfall thresholds less than 100 mm day^{-1}. At the 48-h forecast range, the model performed well only at thresholds below 50 mm day^{-1} and had some skill at 50–100 mm day^{-1}. However, heavy-rainfall events at thresholds over 100 mm day^{-1} were almost unpredictable by the model. Nhu et al. (2017) also used the WRF model to investigate the role of the topography in central Viet Nam on the occurrence of a heavy-rainfall event there in November 1999. In this study, the model with triply-nested domains with Δx of 45, 15, and 5 km and 47 vertical levels well simulated the northeast monsoon circulation, TCs, and the occurrence of heavy rainfall in central Viet Nam. Furthermore, when the topography is removed, the three-day total accumulated rainfall decreased sharply by approximately 75% compared to that in the control experiment with the terrain. Hoa Van Vo (2016) examined the predictability of heavy-rainfall events during the wet seasons of 2008−2012 in the middle section and central highlands of Viet Nam using NWP products from several global models, including the Global Forecasting System (GFS) of NCEP, Global Spectral Model (GSM) of JMA, Navy Operational Global Atmospheric Processing System (NOGAPS) of the US Navy, and the Integrated Forecast System (IFS) of ECMWF. Their results indicated that the IFS and GSM performed better than the GFS and NOGAPS, and the IFS was evaluated the best.

However, all four global models under-estimated rainfall in extreme events. One of the reasons for this under-estimation is that these models are global models, so their resolutions are too coarse for the relatively small study area.

The review above suggests that considerable limitations still exist in forecasting heavy rainfall in central Viet Nam, especially using coarser models. It also indicates that a high-resolution time-lagged ensemble approach may offer some advantages in the prediction of extreme rainfall events, such as a better simulation of local weather conditions, a quicker response to changes in forecast uncertainty in real time, and potentially a longer lead time for hazard preparation. Climatologically, the entire Viet Nam lies in the tropical zone (Fig. 2a), where vigorous but less organized convection often develops in response to local conditions. This region is also prone to the influence and interactions of weather systems spanning a wide range of scales as reviewed. In addition, although central Viet Nam is a small region with the narrowest place only about 80 km in width, it possesses significant topography running in the north-south direction to affect rainfall (Fig. 2a). Hence, a high-resolution CRM with detailed and explicit treatment in cloud microphysics is likely crucial for better QPFs for heavy rainfall in central Viet Nam.

Given the above review and analysis, the scientific hypotheses are proposed: Storm-scale processes and convection were important in the D18 event. However, both global and mesoscale models with a grid size down to 6 km × 6 km are not good enough for heavy-rainfall QPF without cloud-resolving capability (Fig. 1). Therefore, it is hypothesized that at higher resolution, the cloud-resolving time-lagged ensemble system (using the CReSS model) can improve the QPFs of this event at the short range. Additionally, this approach may also be able to extend the lead time of decent QPF beyond the short range. So, the goals of the study are to: 1) examine the hypothesis above, 2) investigate the (practical) predictability of this event through a series of time-lagged ensemble predictions, including whether a decent QPF can be made at a longer lead time, and 3) identify important factors leading to this event, including the lead time of the signals of these factors, using the ESA method. The rest of this paper is organized as follows. Section 2 describes the data, model,

191 and methodology used in the study. The model results are presented and evaluated in
192 Section 3. Finally, conclusions are offered in Section 4.

193 **2 Data and methodology**

194 2.1 Data

195 2.1.1 Model validation

196 *2.1.1.1 In-situ observation data*

197 The daily in-situ rainfall observations (12:00–12:00 UTC, i.e., 19:00–19:00 LST) from 8
198 to 12 December 2018 at 69 automated gauge stations across central Viet Nam are used for
199 case overview and verification of model results. This dataset is provided by the Mid-
200 Central Regional Hydro Meteorological Center, Viet Nam. The spatial distribution of these
201 gauge stations is depicted in Fig. 2b.

202 *2.1.1.2 The Global Precipitation Measurement (IMERG Final Run V07) data*

203 The Global Precipitation Measurement (GPM) is a joint international mission between the
204 National Aeronautics and Space Administration (NASA) and the Japan Aerospace
205 Exploration Agency (JAXA), employing a satellite network for advanced global rain and
206 snow observations. The GPM *IMERG Final Run* is a research-level product which is
207 created by intercalibrating, merging, and interpolating "all" satellite microwave
208 precipitation estimates along with microwave-calibrated infrared (IR) satellite estimates,
209 analyses from precipitation gauges, and potentially other precipitation estimation
210 methodologies at fine spatial and time scales. The horizontal resolution of this dataset is
211 $0.1° \times 0.1°$ latitude–longitude and the time interval is every 30 minute (Huffman et al.
212 2020). In this study, we used this satellite data (version 7) to verify rainfall distribution
213 over the coastal sea due to the limitation of the gauge network, where observations exist
214 only inland as shown in Fig. 2b. The GPM IMERG data span from 12:00 UTC 8 to 12:00
215 UTC 11 December 2018 and are used to analyze the D18 event as well as the rainiest day
216 of this event (10 December).

 2.1.1.3 The NCEP GDAS/FNL global tropospheric analyses data

218 The present study used this dataset (version d083003) to verify initial data and model

219 outputs. The NCEP FNL analysis is an operational global gridded analysis and is freely

220 provided by the NCEP. The horizontal resolution of this dataset is $0.25° \times 0.25°$ latitude–

221 longitude with 26 levels extending from the surface to 10 hPa. The temporal interval is 6

222 h. The variables used in this study include the zonal and meridional wind components,

223 relative humidity, and vertical velocity at 925 hPa covering the case period from 18:00

224 UTC 4 to 12:00 UTC 9 December 2018.

225 2.1.2 The added values of CReSS ensemble

226 *2.1.2.1 The International Grand Global Ensemble retrieval*

227 In this study, we used the global model predictions to analyze the predictability of the D18

228 event. The International Grand Global Ensemble (TIGGE) retrieval is a key component of

229 The Observing System Research and Predictability Experiment (THORPEX) research

230 program, whose aim is to accelerate the improvements in the accuracy of 1-day to 2-week

231 high-impact weather forecasts. The TIGGE retrieval provides not only deterministic

232 forecast data but also ensemble prediction datasets from major centers, including NCEP of

233 the USA, ECMWF of the European countries, and JMA of Japan, since 2006. This dataset

234 has been used for a wide range of research studies on predictability and dynamical

235 processes. the variables utilized included total precipitation and surface winds (at 10-m

236 height) from NCEP, ECMWF, and JMA at 6-h intervals during the data period from 12:00

237 UTC 8 to 12:00 UTC 11 December 2018 (as shown in Figs. 1a-c). The link to this dataset

238 is placed in the "code and data availability" section.

239 2.2.1 Model description and experiment setup

240 We used the Cloud-resolving Storm Simulator (CReSS) developed by Nagoya University,

241 Japan (Tsuboki and Sakakibara, 2002, 2007). This is a non-hydrostatic and compressible

242 cloud model, designed for simulation of various weather events at high (cloud-resolving)

243 resolution. In the model, the cloud microphysics is treated explicitly at the user-selected

244 degree of complexity, such as the bulk cold-rain scheme with six species: vapor, cloud

245 water, cloud ice, rain, snow, and graupel (Lin et al., 1983; Cotton et al., 1986; Murakami,

246 1990, 1994; Ikawa and Saito, 1991). Other subgrid-scale processes parameterized, such as

247 turbulent mixing in the planetary boundary layer and physical options for surface

248 processes, including momentum/energy fluxes, shortwave and longwave radiation, are

249 summarized in Table 1.

250 For the initial and boundary conditions (IC/BCs), the NCEP GFS analyses and

251 deterministic forecast runs, executed every 6 h at 00:00, 06:00, 12:00, and 18:00 UTC daily

252 (dataset ds084.6), were used to drive the CReSS model predictions. The horizontal

253 resolution of the data is $0.25° \times 0.25°$, and 26 of vertical levels, and the forecast fields are

254 provided every 3 h from the initial time out to a range of 192 h. The data link is also placed

255 in the "code and data availability" section.

256 To evaluate of the predictability of the D18 event using an ensemble time-lagged high-

257 resolution system and investigate the ensemble sensitivity of variables for the rainfall, 29

258 experiments were performed. The first member was initialized at 12:00 UTC on 3

259 December and the last one at 12:00 UTC on 10 December 2018. Between them, a new

260 member was initialized every 6 h and all members have a simulation length of 192 h. All

261 experiments used a single domain at 2.5 km horizontal grid spacing and a dimension in (x,

262 y, z) of $912 \times 900 \times 60$ grid points (Table 1, cf. Fig. 2). As mentioned above, the NCEP

263 GFS was used as the IC/BCs of the CReSS model.

264
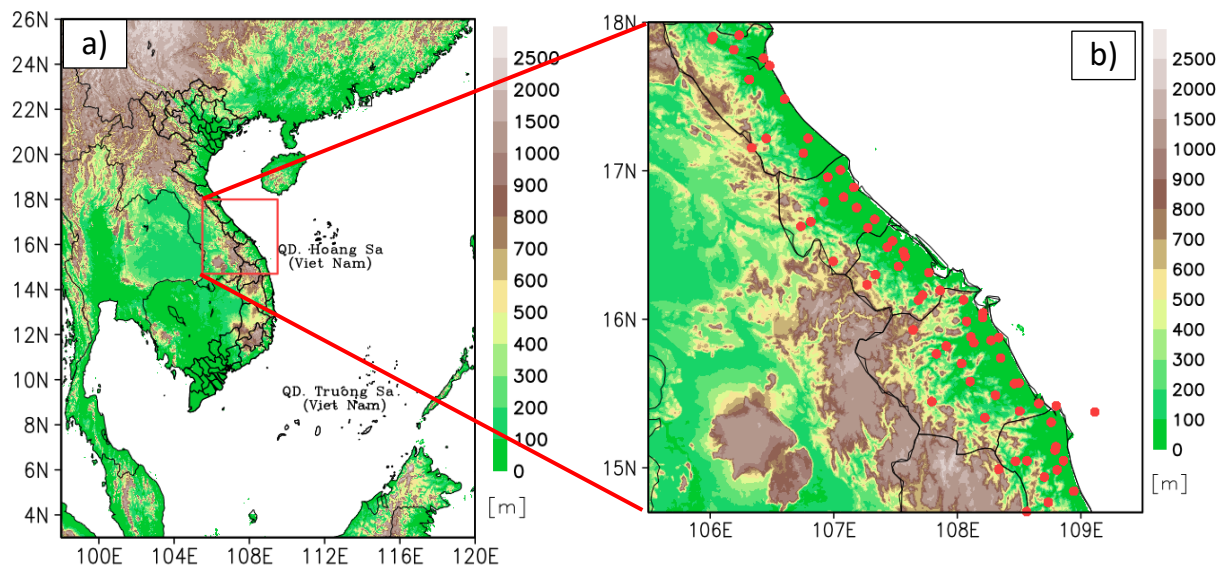
265 **Figure 2**. (a) The simulation domain of the CReSS model and topography (m, shaded)

266 used in the study. The red box marks the study area. (b) The distribution of the

267 observation stations (red dots) in the study area.

268

269 Table 1. The basic information of experiments.

Domain and Basic setup	
Model domain	3°–26°N; 98°–120°E
Grid dimension (x, y, z)	912 × 900 × 60
Grid spacing (x, y, z)	2.5 km × 2.5 km × 0.5 km*
Projection	Mercator
IC/BCs (including SST)	NCEP GDAS/FNL Global Gridded Analyses and Forecasts (0.25° × 0.25°, every 6 h, 26 pressure levels)

Topography (for CTRL only)	Digital elevation model by JMA at (1/120)° spatial resolution
Simulation length	192 h
Output frequency	1 hour
Model physical setup	
Cloud microphysics	Double-moment Bulk cold-rain scheme (six species, Lin et al., 1983; Cotton et al., 1986; Murakami, 1990, 1994; Ikawa and Saito, 1991)
PBL parameterization	1.5-order closure with prediction of turbulent kinetic energy (Deardorff, 1980; Tsuboki and Sakakibara, 2007)
Surface processes	Energy and momentum fluxes, shortwave and longwave radiation (Kondo, 1976; Louis et al., 1982; Segami et al., 1989)
Soil model	41 levels, every 5 cm deep to 2 m

270 * The vertical grid spacing (Δz) of CReSS is stretched (smallest at bottom) and the

271 averaged value is given in the parentheses

272 2.3 Verification of model rainfall

273 In order to verify model-simulated rainfall, some verification methods are used, including

274 (1) visual comparison between the model and the observation (from the 69 automated

275 gauges over the study area), and (2) objective verification using categorical skill scores at

276 various rainfall thresholds from the lowest at 0.05 mm up to 900 mm for three-day total.

277 These scores are presented below along with their formulas and interpretation. To apply

278 these scores at a given threshold, the model and observed value pairs at all verification

279 points N (gauge sites here) are first compared and classified to construct a 2×2 contingency

280 table (Wilks, 2006). At any given site, if the event takes place (reaching the threshold) in

281 both model and observation, the prediction is considered a hit (*H*). If the event occurs only

282 in observation but not the model, it is a miss (*M*). If the event is predicted in the model but

283 not observed, it is a false alarm (*FA*). Finally, if both model and observation show no event,

284 the outcome is correct rejection (*CR*). After all the points are classified into the above four

285 categories, the categorical scores can be calculated by their corresponding formula as:

286 Bias Score (BS) = $(H + FA)/(H + M)$, (1)

287 Probability of Detection (POD) = $H/(H + M)$, (2)

288 False Alarms Ratio (FAR) = $FA/(H + FA)$, (3)

289 Threat Score (TS) = $H/(H + M + FA)$. (4)

290 The values of TS, POD, and FAR are all ranged from 0 to 1, and the higher the better for

291 both TS and POD, but the opposite for FAR. For BS, its possible value can vary from 0 to

292 *N* and indicate overestimation (underestimation) by the model for the events if greater than

293 (less than) unity.

294 2.3.1 The Similarity Skill Score

295 In addition to the categorical scores, the Similarity Skill Score (SSS, Wang et al., 2022) is

296 also applied to evaluate the model rainfall results, as

297
$$\text{SSS} = 1 - \frac{\frac{1}{N}\sum_{i=1}^{N}(F_i - O_i)^2}{\frac{1}{N}\sum_{i=1}^{N}F_i^2 + \frac{1}{N}\sum_{i=1}^{N}O_i^2}, \quad (5)$$
298

299 where *N* is the total number of verification points as before, and F_i is the forecast rainfall

300 amount and O_i is the observed value at the *i*th point among *N*, respectively. The SSS is a

301 measure against the worst mean squared error (MSE) possible. The formula shows that a

302 forecast with perfect skill has an SSS of 1, while a score of 0 means zero skill when the

303 model rainfall does not overlap with the observation anywhere.

304 2.3.2. The ensemble spread (standard deviation)

The ensemble spread is a measure of the difference among the members about the ensemble mean, and one suitable parameter is the standard deviation (SD). In other words, the ensemble spread reflects the diversity of all possible outcomes. Hence, the ensemble spread is often applied to describe the magnitude of the forecast errors. For example, a small spread indicates high theoretical forecast accuracy (and low uncertainty), and vice versa for a large spread. Using the SD, the spread is computed by the formula below:

$$\mathrm{SD} = \sqrt{\frac{\sum_{i=1}^{n}(x_i - \mu_x)^2}{n-1}} \quad , \tag{6}$$

where x_i is the predicted value of member i for the variable x, μ_x is the ensemble mean, and n is the total number of ensemble members, respectively.

2.3.3. Ensemble Sensitivity Analysis

As mentioned above, an ensemble forecast is a set of forecasts produced by many separate forecasts typically with different initial conditions. Moreover, as we know, NWP outcomes are often sensitive to small changes in ICs and the sensitivity analysis is considered a method to improve forecasts through targeting observations. Hence, this study used the ESA method introduced by Ancell and Hakim (2007) to examine how a forecast variable responds to changes in ICs. The ensemble sensitivity is computed by the formula:

$$\frac{\partial R}{\partial x_t} = \frac{COV(R, x_t)}{VAR(x_t)} . \tag{7}$$

Here, the response function R is chosen to be the areal-mean 24-h accumulated rainfall in central Viet Nam (15.5°-16.3°N, 107.9°-108.6°E) on the rainiest day, from 12:00 UTC 9 to 12:00 UTC 10 December 2018. The starting time of this period, i.e., 12:00 UTC 9 December, is defined as t_0. Various scalar variables are considered for x_t, at a time from 48 h earlier (t_{-48}, or 12:00 UTC 7 December) to t_0 at 24-h intervals. The COV is the covariance of R and x_t, and VAR is the variance of x_t, respectively.

329   Since the analysis in part 1 has identified that the D18 event was caused by the combined

330   effect between the atmospheric disturbances at lower levels, such as the cold surge and

331   easterly wind, and the topography, the ESA herein has been applied to selected variables

332   at surface, near-surface, and mid-tropospheric levels to assess the sensitivity of the rainfall

333   field to ICs and its predictability. In order to facilitate the comparison among the impacts

334   of different variables, this study normalized ESA results by using the standardized anomaly

335   in the denominator of Eq. (7) and expressed them as the change in R (in mm) in response

336   to an increase in x_t by one SD in subsequent sections.

3 Model results

3.1 Time-lagged 24-h QPFs by the CReSS model

339   In this section, time-lagged forecasts targeted for the 24-h period from 12:00 UTC on 9 to

340   12:00 UTC on 10 December in the D18 event by the 2.5-km CReSS model are presented

341   and evaluated. This 24-h period is chosen because it is the rainiest day with in-situ

342   observation exceeding 600 mm at some stations (Fig. 3 OBS). Figure 3 shows 25 possible

343   scenarios of 24-h rainfall and average surface winds over the target period produced by the

344   lagged runs every 6 h, with the earliest initial time at 12:00 UTC 3 December and the latest

345   one at 12:00 UTC 9 December 2018. This is true for a well calibrated ensemble, only. It is

346   immediately clear that several members made a rather good 24-h QPF not only in amounts,

347   but also in rainfall location and spatial distribution. These include most members starting

348   during 8-9 December, and also an impressive member from 18:00 UTC 4 December. In

349   this latter run, a reasonably good QPF was produced at a rather long lead time, almost five

350   days (114 h) prior to the beginning of the target period. A common feature among these

351   good members is that they all captured the direction and magnitude of surface winds quite

352   well. On the other hand, most other members were less ideal in their QPFs when initialized

353   before 06:00 UTC on 7 December at lead times beyond two days (before the target period).

354   In general, they also did not predict the surface winds well enough.

355
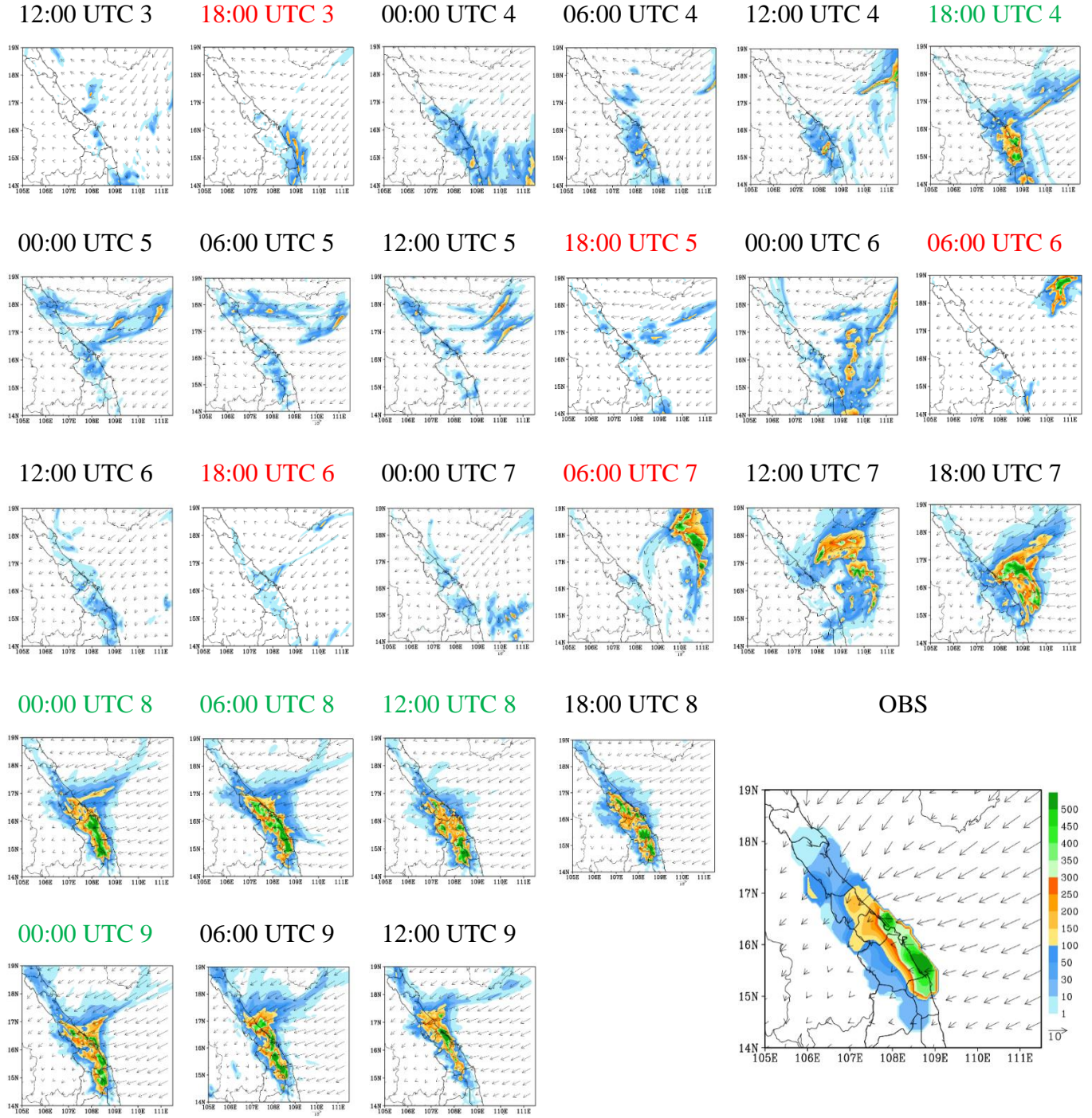
Figure 3. The predicted 24h accumulated rainfall (mm, shaded, scale on the right of panel OBS) and the mean surface horizontal wind (ms⁻¹, vector, reference length at panel OBS) on 10 December 2018 (from 12:00 UTC 9 December to 12:00 UTC 10 December 2018). The green color mark good members and the red color marks bad members. In OBS, 24h

in-situ observed rainfall (mm, shaded) and the surface wind derived from ERA5 data (ms^{-1}, vector), adapted from Fig. 12f of Wang and Nguyen (2023).

Furthermore, as we know, ensemble weather forecasts are a set of forecasts from multiple members that represent the range of future weather possibilities, and the simplest way to use them is through the ensemble mean, which emphasizes the features that the members agree upon. In order to see how well the 2.5-km CReSS can predict the D18 event with the time-lagged strategy in terms possible scenarios of 24-h accumulated rainfall for 10 December, lagged runs are grouped based on their range of initial times in Fig. 4. It can be clearly seen that the rainfall predictions by the fifth four (executed between 12:00 UTC 7 and 06:00 UTC 8 December) and the sixth four members (between 12:00 UTC 8 and 06:00 UTC 9 December) are quite similar to the observation, not only in rainfall amount but also in the locations of concentrated rainfall. For other subgroups, the rainfall was much lower than the observation in their scenarios. In which, the rainfall accumulations from the third (12:00 UTC 5 to 06:00 UTC 6 December) and fourth four (12:00 UTC 6 to 06:00 UTC 7 December) members are the lowest. One relevant assessment to the outcome of these eight runs is that none of them predicted the surface wind field well enough at their ranges (beyond three days), as discussed previously. On the other hand, the mean rainfall from the second four members (12:00 UTC 4 to 06:00 UTC 5 December) is the best among all subgroups at the extended range due to a single good forecast initialized at 18:00 UTC on 4 December [cf. Fig. 3 (18:00 UTC 4)].
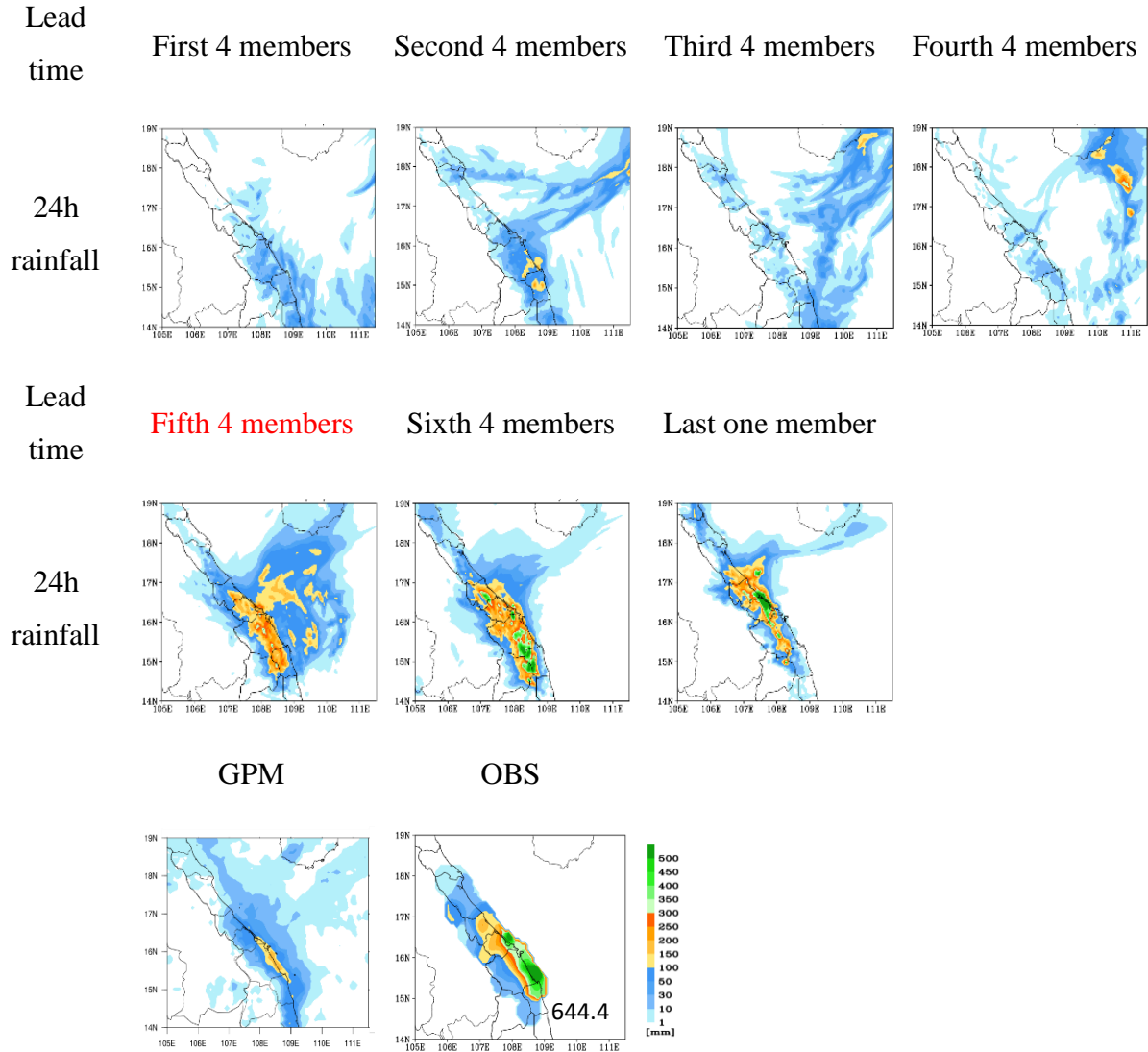
Figure 4. The predicted 24h rainfall by subgroup members, 24h accumulated rainfall by the Global Precipitation Measurement (GPM) estimate (IMERG Final Run product), 24h observed rainfall (mm, peak amount labeled at the lower-right corner) for the period of 12:00 UTC 9 December – 12:00 UTC 10 December 2018 as labelled. The same color bar (lower right) is used for all panels.

Besides the evaluation on time-lagged results using batches of successive runs (every 4 members) as presented above, this study also grouped the members using different ensemble sizes based on their behavior in order to better assess the temporal evolution of

394 forecast uncertainty and event predictability as the lead time shortened. Particularly, the 25

395 members were divided into several subgroups as shown in Fig. 5, including the first eight

396 members (those executed during 12:00 UTC 3–06:00 UTC 5 December), the middle eight

397 members (runs between 12:00 UTC 5 and 06:00 UTC 7 December), the last nine members

398 (12:00 UTC 7–12:00 UTC 9 December), and the last five members (12:00 UTC 8–12:00

399 UTC 9 December), respectively. In other words, the last five members were those executed

400 within 24 h (1 day) prior to the beginning of the target period, and so on.

401 In Fig. 5, it is clear that both the ensemble means from the last five and the last nine

402 members compare quite favorably to the observation, not only in the accumulated amount

403 but also in spatial distribution of rainfall. This indicates that the model could produce QPFs

404 at fairly good quality and rather consistently since the time as early as roughly 48 h prior

405 to the commencement of the rainfall event (also Fig. 3). These two sub-groups within the

406 short range gave much better quality in QPFs than the other sub-groups executed before

407 them at longer lead times, including the first eight, middle eight, and all 25 members.

408 In terms of skill scores, for example, the mean QPF by the last five members have TS =

409 0.4, POD = 0.8, BS = 1.5, and FAR = 0.5 at 100 mm (per 24 h), while the last nine members

410 give similar scores of TS = 0.5, POD = 0.8, BS = 1.4, and FAR = 0.5 (Figs. 6a-d),

411 respectively. On the contrary, the mean QPFs from both the first and middle eight members

412 only yield zero scores in TS, POD, and BS with no skill in FAR at 100 mm (and above),

413 obviously due to not enough rainfall in central Viet Nam in most of their members. At 200

414 mm (per 24 h), similarly, the last five members (TS = 0.2, POD = 0.4, BS = 1.4, and FAR

415 = 0.7) and the last nine members (TS = 0.3, POD = 0.5, BS = 1.2, and FAR = 0.6) again

416 produce much better scores in QPFs, compared to no skill in all four scores in QPFs from

417 the middle eight, first eight, and all 25 members (Figs. 6a-d). In SSS, the mean from the

418 last nine members exhibits the highest score (0.64), the middle eight members have the

419 lowest score (0.04), and the mean from all 25 members is 0.43 (Fig. 6e).

420

421
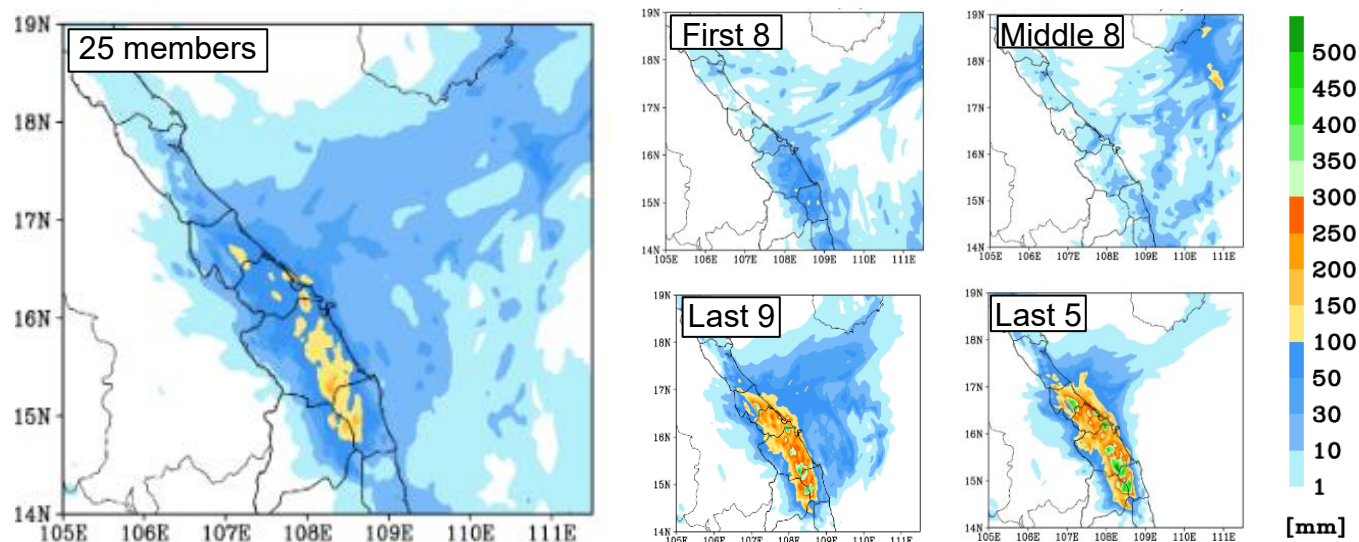
Figure 5. Ensemble mean rainfall (shaded, scale on the right) from all 25 time-lagged members, executed every 6 h from 12:00 UTC 3 December to 12:00 UTC 9 December, for the 24h period from 12:00 UTC 9 December to 12:00 UTC 10 December.
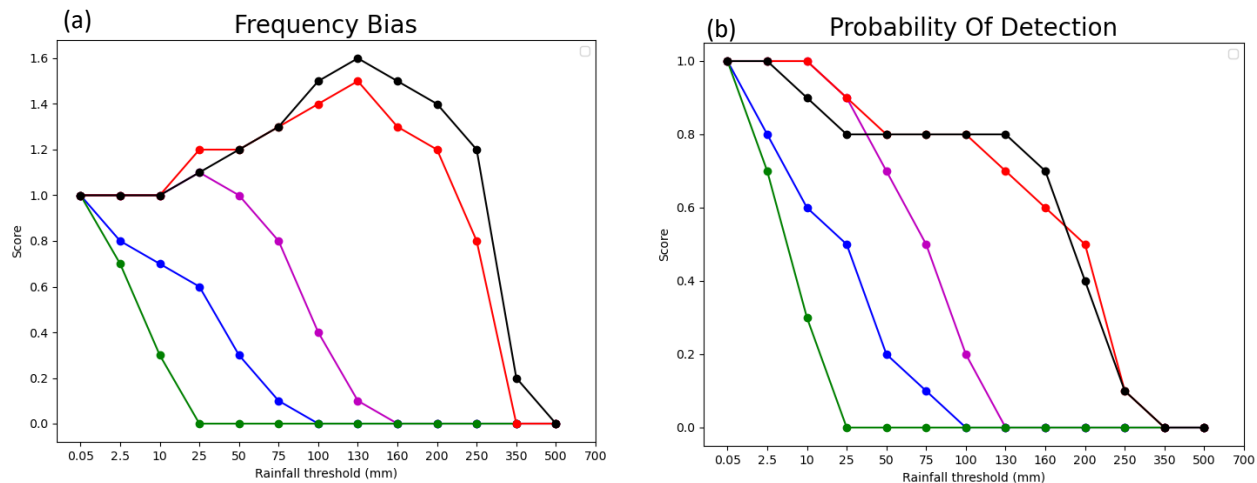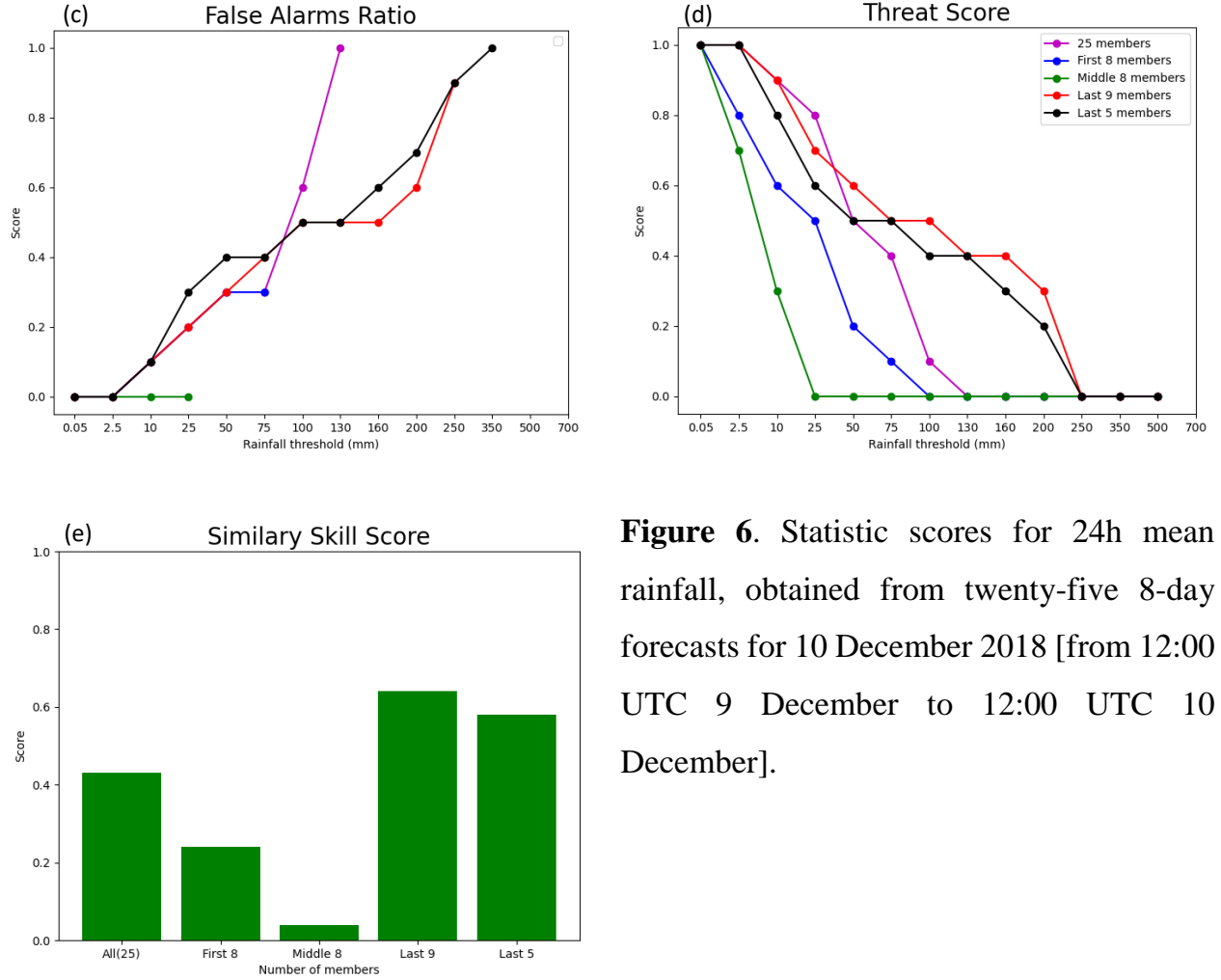
Figure 6. Statistic scores for 24h mean rainfall, obtained from twenty-five 8-day forecasts for 10 December 2018 [from 12:00 UTC 9 December to 12:00 UTC 10 December].

425

However, as indicated by the SD, the spreads in rainfall scenarios in both ensembles from the last five and nine members are quite large (Fig. 7). Thus, while the lagged members can produce a wide range of possible rainfall scenarios for the D18 event, which is the main purpose of an ensemble as reviewed in Section 1, the members often cannot agree on the precise locations of heavy rainfall. Given the small scale of local convection during the event, this result is perhaps anticipated. On the other hand, the maxima in spread are >160 mm in Fig. 7 among the last nine members, perhaps quite reasonable in magnitude compared to the peak amounts of about 400 mm in the ensemble mean. In any case, Figs. 6 and 7 indicate that the predictability of the D18 event changed considerably with time,

435 and the 2.5-km CReSS has a good skill in QPFs inside the short range (≤ 72 h). However,

436 it remains difficult to predict the event successfully at longer lead times.

437

438
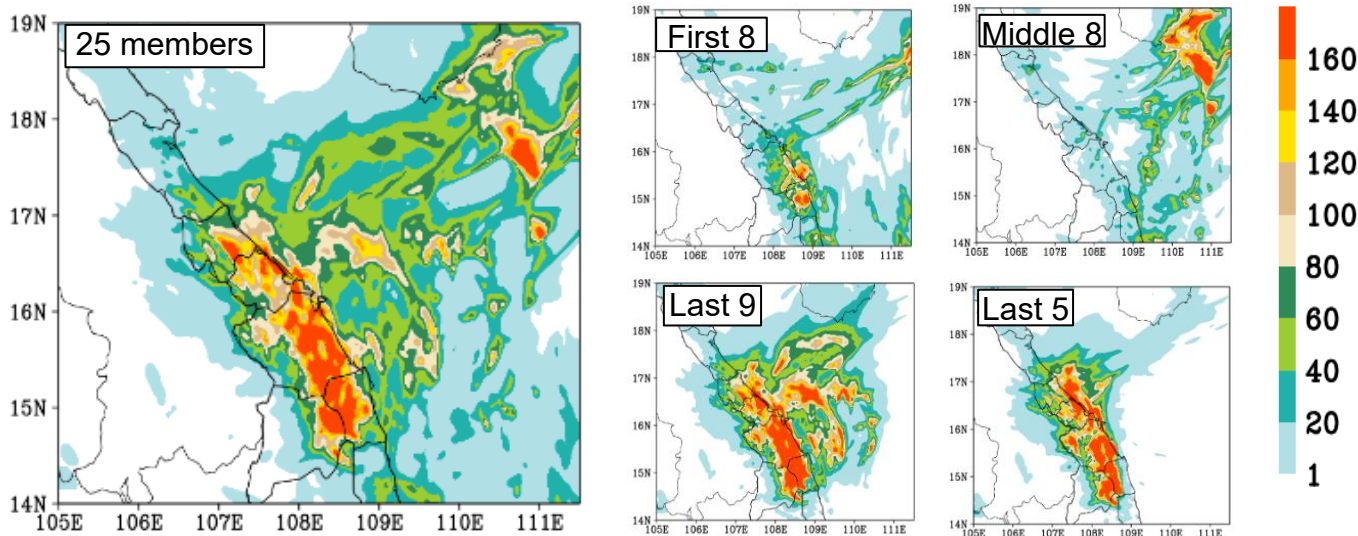
439 **Figure 7**. The spread (shaded, scale on the right) from all 25 time-lagged members,

440 executed every 6 h from 12:00 UTC 3 December to 12:00 UTC 9 December, for the 24h

441 period from 12:00 UTC 9 December to 12:00 UTC 10 December.

442

443 The probability information derived from the sub-ensemble groups at four different rainfall

444 thresholds from 100 to 450 mm is shown in Fig. 8, in which the increase in heavy-rainfall

445 probability in central Viet Nam and thus the predictability of the event with time is also

446 evident. From the first eight members executed at the longest range (≥ 102 h prior to rainfall

447 accumulation), there is only a 10-25% chance in parts of central Viet Nam to receive at

448 least 100 mm of rainfall for 10 December (from 12:00 UTC 9 to 12:00 UTC 10 December).

449 The probability is even lower from the middle eight members (run between 54-96 h prior

450 to target period), as their SSS is the lowest among all sub-ensemble groups and only a

451 couple of the runs could reach 100 mm anywhere inland in central Viet Nam. As the lead

time shortens to inside the short range, the probabilities to have ≥ 100 mm of rainfall increase dramatically, to roughly 70-80 % in the last nine members and further to over 80-90% in the last five members. Due to the contribution from later members, about 20-40% of all 25 members can reach 100 mm inland. Toward higher thresholds, the probabilities decrease in Fig. 8 as expected, so do the areal sizes actually reaching those thresholds (pink contours). At the highest value of 450 mm, the ensembles in general show less than about 20%-30% chance for its occurrence from the last five and last nine members, respectively, and the high probability areas are also slightly more inland than the observed one.
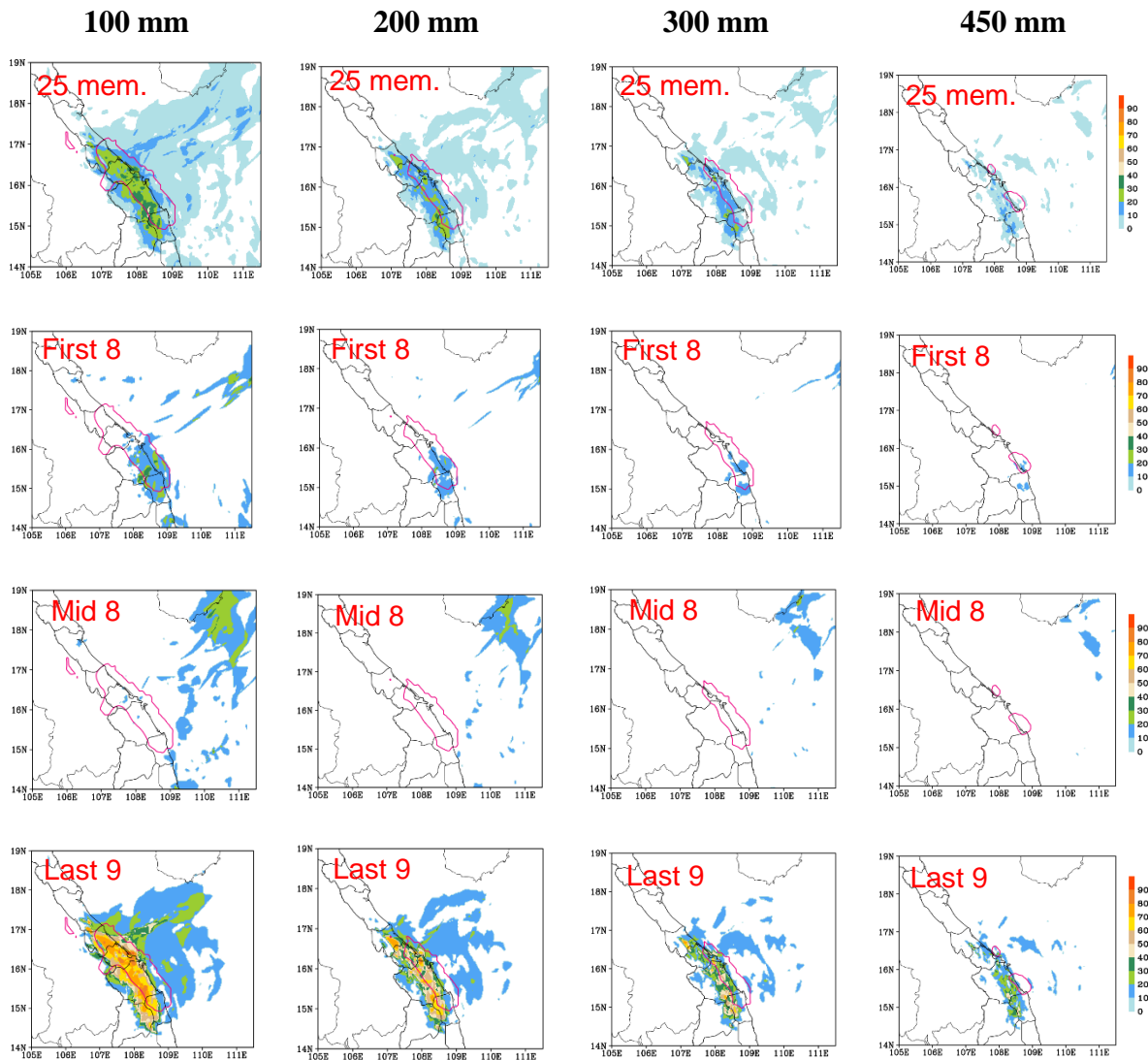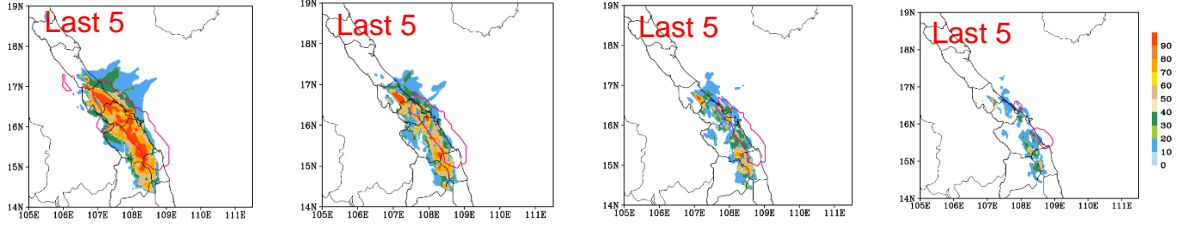
Figure 8. Probability distribution (%; shaded, scale on the right) from all 25 time-lagged members, executed every 6 h from 12:00 UTC 3 December to 12:00 UTC 9 December, reaching thresholds of 100, 200, 300, and 450 mm, for the 24h period from 12:00 UTC 9 December to 12:00 UTC 10 December. The observed areas at the same thresholds are depicted by the pink contours. For each picture, red labeled at the top-left corner show the number of members grouped to calculate the probability distribution.

3.2 Ensemble-based sensitivity analysis

The results in Section 3.1 above reveal that the CReSS model with a horizontal grid size of 2.5 km predicted good QPFs for the rainiest day of the event and performed better than those reviewed in Section 1. Therefore, relying on this good performance, the ESA is carried out in this subsection.

Firstly, five good members (those with initial times at 18:00 UTC on 4, 00:00, 06:00, and 12:00 UTC on 8, and 00:00 UTC on 9 December) and five bad ones (those ran at 18:00 UTC on 3, 18:00 UTC on 5, 06:00 and 18:00 UTC on 6, and 06:00 UTC on 7 December) are chosen and by using their differences (good minus bad members), Fig. 9 shows that the main reason for the significantly different forecast outcomes lies in differences in the input datasets (i.e., IC/BCs). Specifically, the surface easterly winds were much stronger and the relative humidity much higher surrounding central Viet Nam and its upstream areas in the GFS forecast data valid at 12:00 UTC on 9 December (used as BCs in CReSS runs) in the good members than in the bad ones (Fig. 9a). Subsequently, the good CReSS members produced much more rainfall in central Viet Nam (Fig. 9b). These factors were also identified as crucial for the extreme rainfall in the D18 event in Part 1.

483
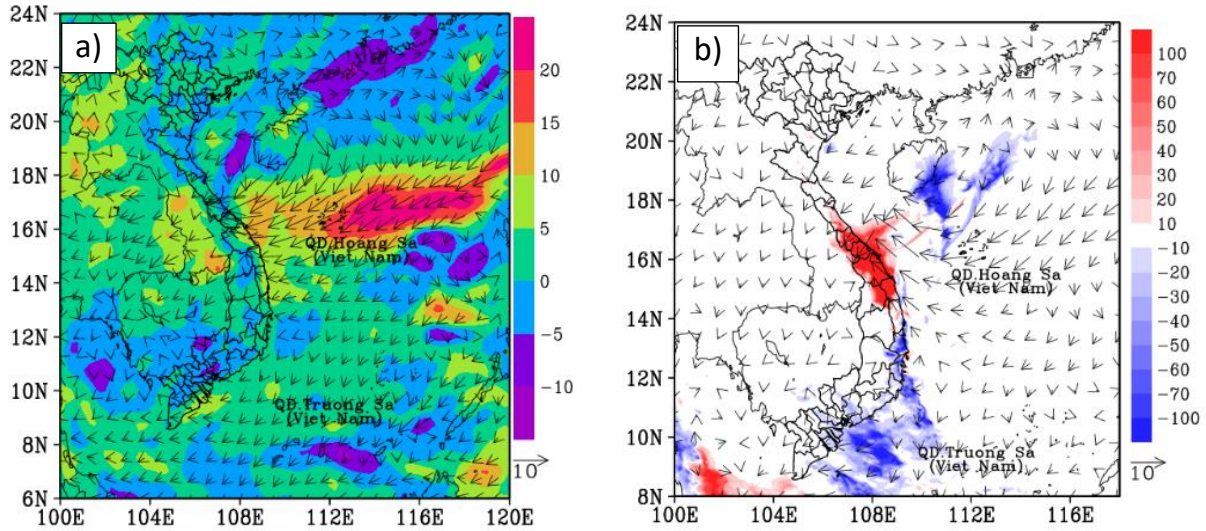
Figure 9. The difference in (a) input data (boundary conditions) and (b) CReSS output between averaged 5 good members (members ran at 18:00 UTC 4, 00:00 UTC 8, 06:00 UTC 8, 12:00 UTC 8, 00:00 UTC 9) and 5 bad members (members ran at 18:00 UTC 3, 18:00 UTC 5, 06:00 UTC 6, 18:00 UTC 6, 06:00 UTC 7). For input data, relative humidity (%, shaded) and surface wind (ms^{-1}, vector) at 12:00 UTC December 9 2018. For CReSS output, 24-h accumulated rainfall (mm, shaded) and surface wind (ms^{-1}, vector).

Meanwhile, Fig. 10 shows the difference in the evolution of synoptic-scale patterns (features) zoomed into the study area. To be more specific, Fig. 10a depicts the difference (CReSS output minus NCEP FNL analysis) in the horizontal wind and vertical velocity between the averages of the 5 good members and the NCEP FNL analysis at 925 hPa at 12:00 UTC 9, and it is small although each member was initialized at a different lead time. It implies that these members captured well the evolution of weather patterns of this event. Additionally, the model vertical velocity is seen to be stronger than the NCEP FNL data. Therefore, these members produced the rainfall closer to the observation with the presence of complex terrain in the study area. On the contrary, bad members did not capture the evolution of weather patterns well enough (Fig. 10b), and they could not produce good QPFs as a result.

501 Furthermore, Fig. 10d indicates very small differences in the IC of the member that was

502 initialized at 18:00 UTC 4 to the FNL analysis (thus suggesting smaller errors), especially

503 over the study area. From this initial data, the evolution of weather patterns in this CReSS

504 run also agreed well with the analyses during the first three days (not shown), and the

505 differences remained relatively small even at 12:00 UTC 9, at a lead time of roughly 5 days

506 (Figs. 10e,f,g). Compare to this, a bad member initialized at 18:00 UTC 6 (at a shorter lead

507 time by 2 days) exhibited somewhat larger differences in the initial state in relation to the

508 NCEP FNL analysis (Fig. 10h). This difference then led to larger and more evident

509 differences in weather patterns, as seen in Figs. 10 i, j, k by this particular member that

510 performed worse in QPFs (member ran at 18 UTC 06). The results here not only indicate

511 that it is still possible to have good rainfall forecasts at a lead time up to 5 days, but also

512 show some predictability by a cloud-resolving model at such long lead times.

513

514

515

516
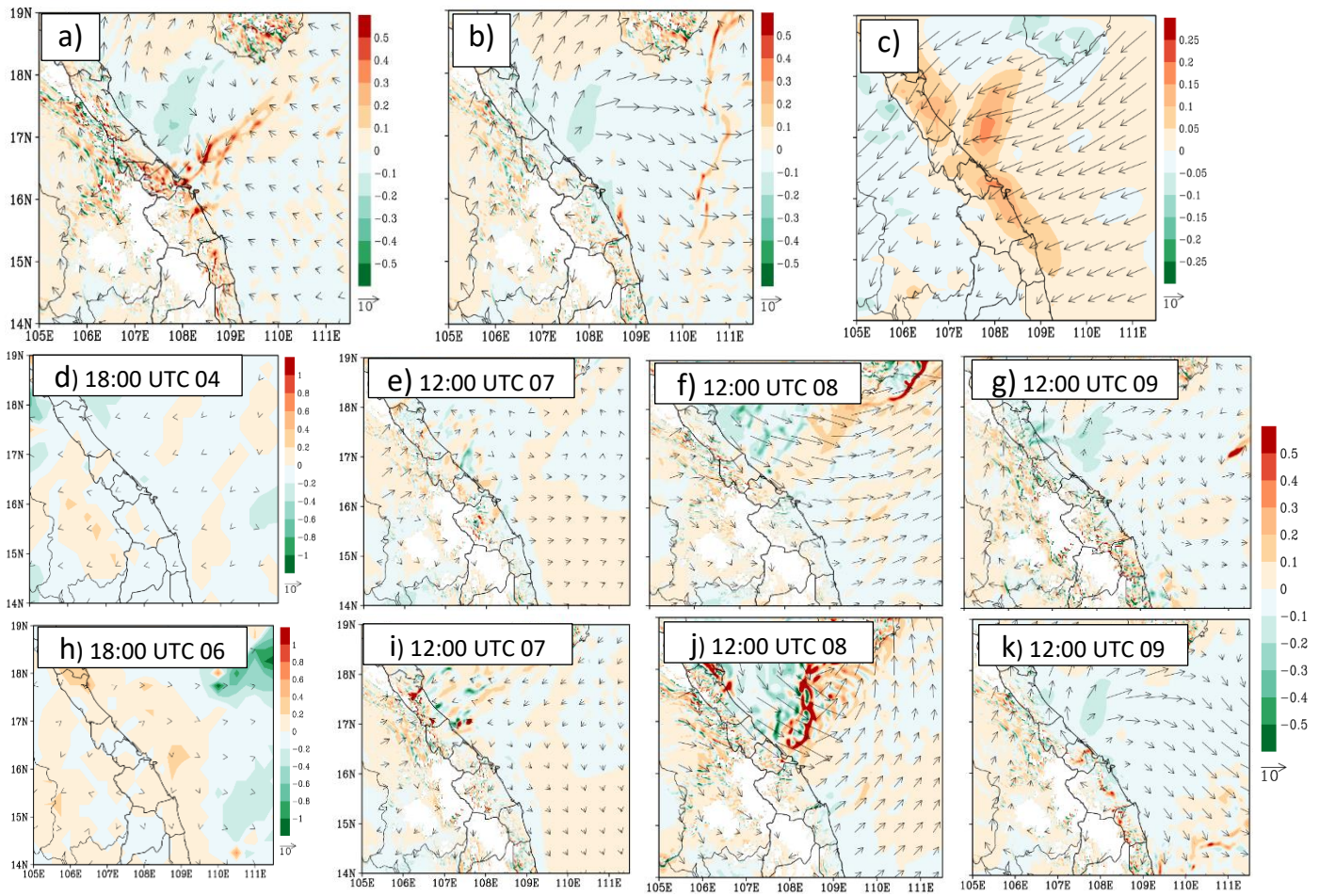
Figure 10. The difference in the horizontal wind (ms^{-1}, vector, reference length at the low-right corner of the panel), and vertical velocity (ms^{-1}, shaded, the reference color scale is on the right of panel) between (a) averaged 5 good members and (b) averaged 5 bad members and the NCEP FNL analysis data at 925 hPa and at 12 UTC 09. (c) The NCEP FNL analysis horizontal wind (ms^{-1}, vector, reference length at the low-right corner of the panel) and vertical velocity (ms^{-1}, shaded) at 925 mb and at 12 UTC 09. (d) The difference in the horizontal wind (ms^{-1}, vector, reference length at the low-right corner of the panel), and relative humidity (%, shaded, the reference color scale is on the right of panel) between the initial data of a good member at a longer lead time (at 1800 UTC 4 Dec) and the NCEP FNL analysis data at 925 hPa. (e), (f), and (g) present the difference in the evolution of weather features with time by this good member. (h) as in (d) but for a bad member (member ran at 1800 UTC 6 Dec). (i), (j) and (k) as in (e), (f), and (g), respectively, but for

529   mentioned bad member. Compared variables are horizontal wind at 925 hPa (ms^{-1}, vector,

530   reference length at the low-right corner of the panel) and vertical velocity (ms^{-1}, shaded,

531   the reference color scale is on the right of panel). The NCEP FNL analysis horizontal wind

532   (ms^{-1}, vector, reference length at the low-right corner of the panel) and vertical velocity

533   (ms^{-1}, shaded) at 925 mb.

534   Additionally, the above results also reaffirm that very small differences in the initial data

535   can lead to a vastly different outcome, especially as the forecast range increases, in extreme

536   rainfall events (such as the D18 event) that involve highly nonlinear deep convection. As

537   pointed out in Part 1, the low-level wind convergence led to moisture convergence and

538   these conditions played a crucial role in the D18 event. The southward movement of the

539   low-level wind convergence also dictated the movement of the convective rainband during

540   the event. Therefore, the ESA was applied on relevant variables, including the horizontal

541   wind and mixing ratio of water vapor. The quantitative results are shown in Figs. 11-13

542   and presented below.

543   Figure 11 shows the sensitivity of mean 24-h total rainfall inside the green box in central

544   Viet Nam (R) to zonal (u) and meridional (v) wind components and water vapor mixing

545   ratio (q_v) at the surface, with the ensemble mean also plotted. It is clear that the sensitivity

546   of rainfall to these variables is lower at longer forecast ranges and becomes higher as the

547   lead time shortens. Specifically, from two days before (t_{-48}) to the starting time of the

548   accumulation period (t_0), the sensitivity of rainfall to u-wind over the SCS and along the

549   coast of central Viet Nam turned more negative, indicating heavier rainfall associated with

550   stronger easterly winds ($u < 0$) near the surface, especially in areas immediately upstream

551   toward t_0 (Figs. 11a-d). The rainfall's sensitivity to v-wind leading to t_0, on the other hand,

552   exhibited a dipole structure in pattern, with negative values to the north-northwest and

553   positive values to the south-southeast across central Viet Nam and the upstream ocean

554   (Figs. 11e-h). This structure indicates a stronger confluence in northeasterly winds over the

555   region in rainier members, consistent with the results in Part 1. In Figs. 11e-h, the increase

556   in v-wind just south of central Viet Nam is particularly evident, from -10 mm per SD (SD

557 = 2 ms^{-1}) at t_{-48} to over +70 mm per SD (SD = 2-4 ms^{-1}) at t_0. Thus, the precipitation amount

558 over central Viet Nam in the D18 event is highly sensitive to the strength and confluence

559 of northeasterly winds near the surface in short-range forecasts. Similarly, the rainfall was

560 also highly sensitive to the water vapor amount and its flux convergence (Figs. 11i-l).
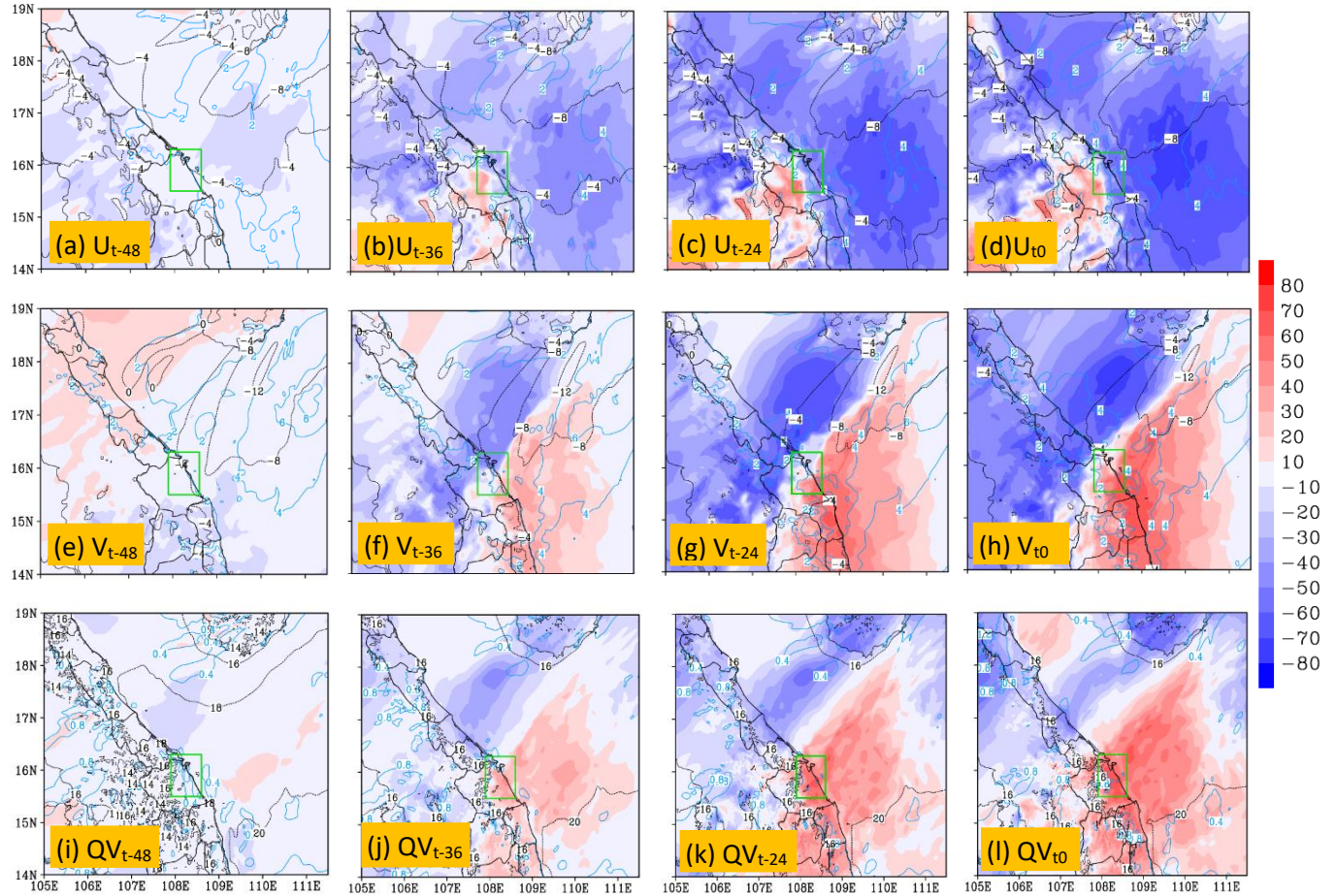
561 **Figure 11**. The sensitivity (mm, per SD, color, scale on the right) of areal-mean 24h

562 accumulated rainfall in central Viet Nam starting from t_0 (i.e., R, averaging area depicted

563 in green box) to surface wind components (ms^{-1}, shaded) and the ensemble mean (contours,

564 every 4 ms^{-1}) and to surface water vapor mixing ratio (r, g kg^{-1}) and its ensemble mean

565 (contours, every 0.06 g kg^{-1}) at different times at 24h intervals from (a) t_{-48} to (f) t_0. The

566 time of t_0 is 12:00 UTC 9 December 2018. In which, (a), (b), (c), (d) for the zonal wind

567 component. (e), (f), (g), (h) for the meridional wind component, and (i), (j), (k), (l) for

568 surface water vapor mixing ratio. The standard deviation is exhibited by the medium blue
569 contours.

570 Slightly higher up at 1476 m (near 850 hPa), where easterly flow prevailed during the D18
571 event (see Fig. 3b in Part 1), the sensitivity of rainfall to *u* and *v* winds exhibits similar
572 spatial patterns (Figs. 12a-h) to those at the surface (Figs. 11a-h), with stronger easterly
573 winds and larger confluence in association with heavier rainfall. Similarly, the rainfall in
574 central Viet Nam is still highly sensitive to mixing ratio at this level, both locally and over
575 the surrounding area scale (Figs. 12i-l), again especially at shorter lead times. At the local
576 scale, this positive correlation presumably is linked to upward transport of moisture, as the
577 ascending motion in convective clouds could become larger at this level (and also more
578 vigorous in rainier members).

579
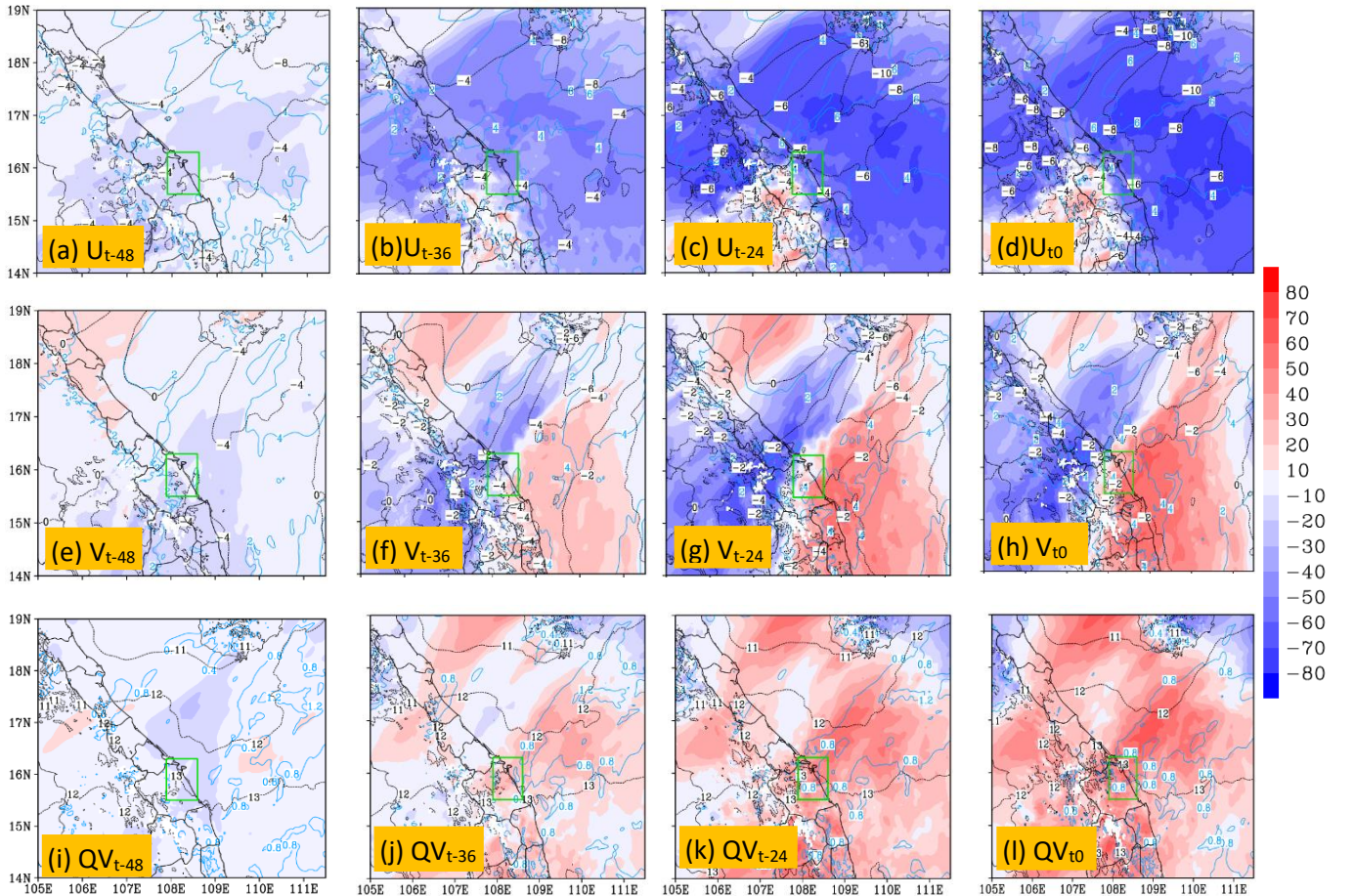
Figure 12. The sensitivity (mm, per SD, color, scale on the right) of 24h accumulated rainfall in central Viet Nam starting from t_0 (i.e., R, averaging area depicted in green box) to the wind components (ms^{-1}, shaded) and the ensemble mean (contours, every 2 ms^{-1}) and to water vapor mixing ratio (r, g kg^{-1}) and its ensemble mean (contours, every 0.4 g kg^{-1}) at attitude of 1476 m and at different times at 24h intervals from (a) t_{-48} to (f) t_0. The time of t_0 is 12:00 UTC 9 December 2018. In which, (a), (b), (c), (d) for the zonal wind component. (e), (f), (g), (h) for the meridional wind component, and (i), (j), (k), (l) for water vapor mixing ratio. The standard deviation is exhibited by the medium blue contours.

At the upper level of 5424 m (near 500 hPa), it is seen that from t_{-48} to t_0, dipole structures developed in the sensitivity patterns of rainfall to both u and v winds (Figs. 13a-h). To u winds, positive sensitivity up to about +70 mm per SD (SD = 2-4 ms^{-1} depending on t) existed to the south, with negative values up to −70 mm per SD (SD = 2-4 ms^{-1}) to the north of central Viet Nam. Meanwhile, positive sensitivity to v-wind appeared to the north and east with negative sensitivity to the south and west of the rainfall area. As the prevailing winds at 500 hPa were southeasterlies over southern Viet Nam and southwesterlies over northern Viet Nam during the D18 event (thus with anticyclonic curvature, see Fig. 3c in Part 1), the above sensitivity patterns, already apparent at t_{-24} (Figs. 13c,g), corresponded to stronger diffluence/divergence and a weaker anticyclone aloft to favor more rainfall. To q_v, positive sensitivity signals up to +70 mm per SD (SD = 1.2 g kg^{-1}) also appeared over the rainfall area at t_{-24} and t_0 (Figs. 13i-l), and the reason is similar to that near 850 hPa in Fig. 12. Overall, the ESA performed in this study indicated clearly that the synoptic pattern that caused the D18 event already developed at times more than 24 h earlier, and this explains why, with a high enough resolution and cloud-resolving capability, the CReSS forecasts could better predict and improve the QPFs inside the short range as shown in Section 3.
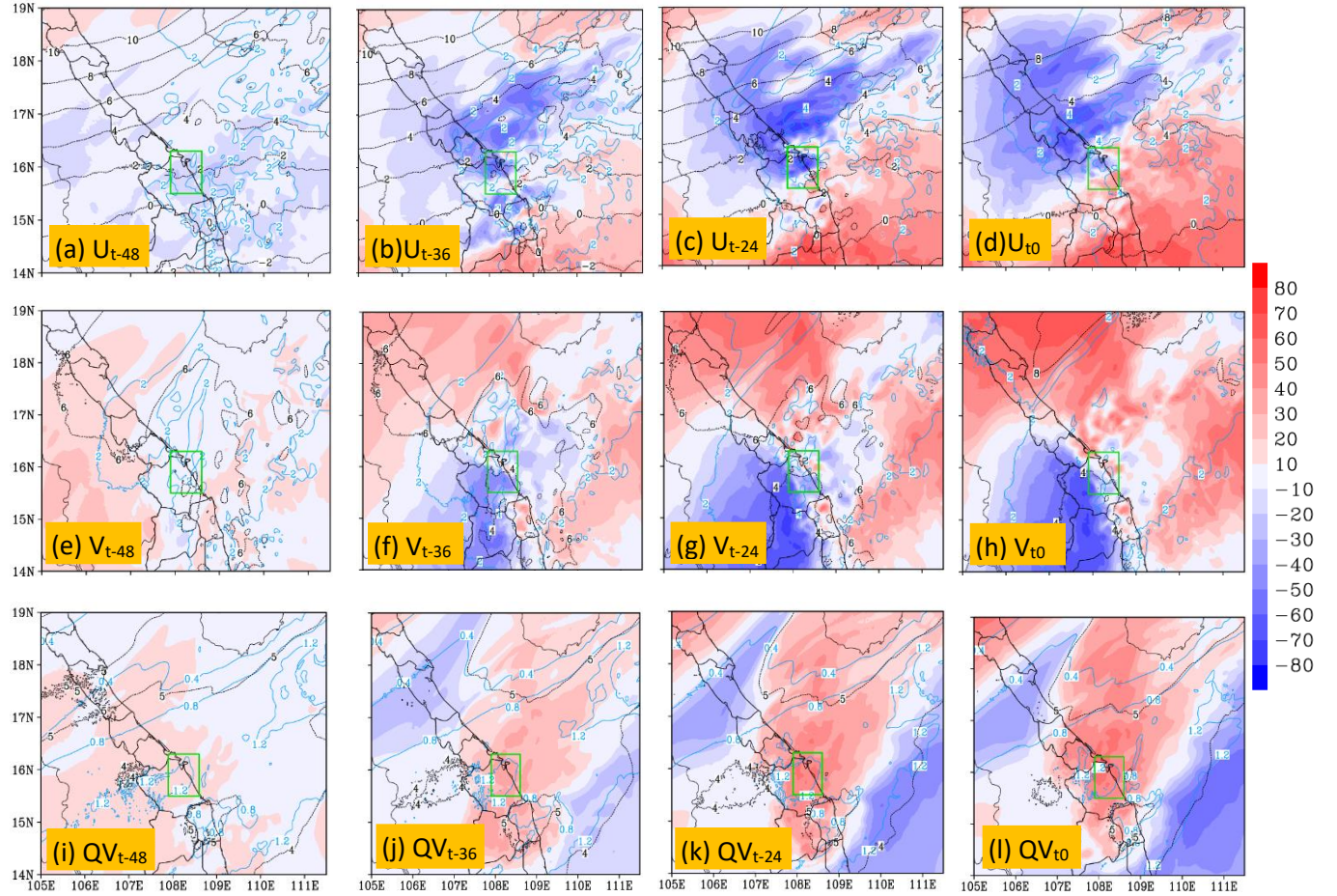
Figure 13. The sensitivity (mm, per SD, color, scale on the right) of 24h accumulated rainfall in central Viet Nam starting from t_0 (i.e., R, averaging area depicted in green box) to the wind components (ms^{-1}, shaded) and the ensemble mean (contours, every 2 ms^{-1}) and to water vapor mixing ratio (r, g kg^{-1}) and its ensemble mean (contours, every 0.4 g kg^{-1}) at attitude of 5424 m and at different times at 24h intervals from (a) t_{-48} to (f) t_0. The time of t_0 is 12:00 UTC 9 December 2018. In which, (a), (b), (c), (d) for the zonal wind component. (e), (f), (g), (h) for the meridional wind component, and (i), (j), (k), (l) for water vapor mixing ratio. The standard deviation is exhibited by the medium blue contours.

4 Conclusion

As high resolution is required in numerical models to predict heavy rainfall more successfully, the present work utilizes a time-lagged high-resolution ensemble forecast

617   system and evaluates how well the D18 event (during 9-12 December 2018) in central Viet

618   Nam can be predicted in advance before its occurrence. Using the CReSS model with a

619   grid size of 2.5 km (912 × 900 in dimension with 60 vertical levels), ensemble forecasts

620   were produced with a total of 29 time-lagged runs at 6-h intervals, each out to a forecast

621   range of 192 h (eight days). Based on the goals raised from the analysis in Part 1, the key

622   findings of this Part 2 study are summarized as follows:

623   The first goal of this study is regarding the scientific hypotheses that at a higher resolution,

624   the cloud-resolving time-lagged ensemble can improve the QPFs of the D18 event at the

625   short range, and may also be able to extend the lead time of decent QPFs beyond the short

626   range. Our evaluation results confirm that this strategy using the CReSS model can

627   effectively improve the QPFs of this event at the short range. Furthermore, the results also

628   demonstrate that a decent QPF for 10 December (the rainiest day) can be made at a longer

629   lead time (initialized at 1800 UTC 4 December), when good initial conditions are provided.

630   About the second goal, our investigation in predictability indicates that the 2.5-km system

631   predicted the rainfall fields on 10 December during the event fairly well, including both

632   the amount and spatial distribution, within the short range at lead times of day 1, 2, and 3.

633   More specifically, the SSS of QPFs at these three ranges are about 0.4, 0.6, and 0.7,

634   respectively, with fairly consistent results among successive runs that indicate a reasonable

635   predictability, despite some spread and disagreement on the precise locations of heavy

636   rainfall. The above good results are due to the model's capability to better predict the

637   conditions in the lower troposphere such as the wind fields.

638   At lead times longer than three days, however, the predictability of the event is lowered

639   due to a higher level of forecast uncertainty, and the quality of QPFs drops with significant

640   under-prediction. Nevertheless, good QPFs are still possible occasionally. At lead time

641   beyond six days, it is challenging to achieve a good QPF at thresholds greater than 100 mm

642   even with a high-resolution model. This is presumably linked to the rapid evolution of

643   atmospheric conditions during such an extreme event surrounding Viet Nam in a tropical

644   environment. In the present study, a CRM is applied to forecast extreme rainfall in central

Viet Nam for the first time. Although still with certain limitations, our results do indicate hope to predict such events successfully beforehand, at least within the short range. Therefore, based on the present work, more studies on the predictability of extreme rainfall in Viet Nam are recommended in the near future.

Regarding the third and final goal, ESA results show that the rainfall is most sensitive to the wind conditions in the lower troposphere leading to the event, with more rain associated with stronger northeasterly to easterly winds and their confluence over central Viet Nam (and the upstream region). Similarly, the rainfall also shows strong sensitivity to the moisture amount, not only at the surface but also further aloft at the upper levels. Besides, ESA also indicates that the synoptic pattern that caused the D18 event already developed at timing earlier in the past. Furthermore, in the ESA, the finer-scale features (convection) are also seen to link to synoptic conditions in their background, implying that it is meaningful to apply ESA to control the perturbations in initial fields.

The key findings in this study underscore that both practical predictability and ESA are intertwined, influencing the design and evaluation of ensemble forecast systems, and potentially applicable to other extreme rainfall events in the same season in Vietnam.

Acknowledgements: This study was supported by the project "*Research on the application of the Cloud-resolving model integrated with the regional numerical model to a 6-hour accumulated quantitative precipitation forecast with 24-48 hours lead time for Mid-Central Viet Nam*", which is funded by the Ministry of Natural Resources and Environment (MONRE) under grant no. TNMT.2023.06.07, and also by the National Science and Technology Council (NSTC) of Taiwan under grants MOST 111-2625-M-003-001, NSTC 112-2625-M-003-001, NSTC 113-2625-M-003-001, and NSTC 113-2111-M-003-001.

Code and data availability. The CReSS model used in this study and its user's guide are available at the model website at http://www.rain.hyarc.nagoya-u.ac.jp/~tsuboki/cress_html/src_cress/CReSS2223_users_guide_eng.pdf (last access: 6

July 2023; Tsuboki and Sakakibara, 2007). The TIGGE data and its information are available at https://confluence.ecmwf.int/display/TIGGE/TIGGE+archive. The NCEP GFS dataset and its description are available at https://rda.ucar.edu/datasets/ds084.1/. The NCEP FNL operational global gridded analysis data and its information is available at https://rda.ucar.edu/datasets/d083003/#.

Author contributions. **Duc Van Nguyen** prepared datasets, executed the model experiments, performed the analysis, and prepared the first draft of the manuscript. **Chung-Chieh Wang** also prepared the first draft and provided the funding, guidance and suggestions during the study, and they participated in the revision of the manuscript. **Kien Ba Truong** provided the funding and participated revising of the manuscript. **Thang Van Vu**, **Pham Thi Thanh Nga**, and **Pi-Yu Chuang** also participated in the revision of the manuscript.

Competing interests. The authors declare that they have no conflict of interest.

References

Ancell, and Hakim, G. J.: Comparing adjoint- and ensemble sensitivity analysis with applications to observation targeting. Mon. Wea. Rev., 135, 4117–4134, doi:10.1175/2007MWR1904.1, 2007.

Cotton, W. R., Tripoli, G. J., Rauber, R. M., and Mulvihill, E. A.: Numerical simulation of the effects of varying ice crystal nucleation rates and aggregation processes on orographic snowfall. J. Appl. Meteorol. Clim., 25, 1658–1680, 1986.

Coleman,A. A., and Ancell, B. C.:Toward the improvement of high-impact probabilistic forecasts with a sensitivity-based convective-scale ensemble subsetting technique. Mon. Wea. Rev., 148, 4995–5014, https://doi.org/10.1175/MWRD-20-0043.1, 2020.

Deardorff, J. W.: Stratocumulus-capped mixed layers derived from a three-dimensional model. Bound.-Lay. Meteorol., 18, 495–527, 1980.

Hu, C.-C., and Wu, C.-C.: Ensemble sensitivity analysis of tropical cyclone intensification rate during the development stage. J. Atmos. Sci., 77, 3387–3405, https://doi.org/10.1175/JAS-D-19-0196.1, 2020.

Hoa, V. V.: Comparative study skills rain forecast the middle part and central highland of several global models (In Viet Namese). Viet Nam journal of Hydrometeorology. V. 667 No. 07 (2016), 2016.

Hohenegger, C., and Schär, C.: Predictability and error growth dynamics in cloud-resolving models. J. Atmos. Sci., 64, 4467–4478, https://doi.org/10.1175/2007JAS2143.1, 2007.

Huffman, G. J., Bolvin, D. T., Braithwaite, D., Hsu, K., Joyce, R., Kidd, C., Nelkin, E.J., Sorooshian, S., Tan, J., Xie, P.: Algorithm Theoretical Basis Document (ATBD) Version 06: NASA Global Precipitation Measurement (GPM) Integrated Multi-Satellite Retrievals for GPM (IMERG). NASA/GSFC, Greenbelt, MD, USA, https://gpm.nasa.gov/sites/default/files/2020--05/IMERG_ATBD_V06.3.pdf, 2020.

Ikawa, M. and Saito, K.: Description of a non-hydrostatic model developed at the Forecast Research Department of the MRI, MRI Technical report 28, Japan Meteorological Agency, Tsukuba, Japan, ISSN: 0386-4049, 1991.

Kerr, C. A., Stensrud, D. J. and Wang, X.: Diagnosing convective dependencies on near-storm environments using ensemble sensitivity analyses. Mon. Wea. Rev., 147, 495–517, https://doi.org/10.1175/MWRD-18-0140.1, 2019.

Kondo, J.: Heat balance of the China Sea during the air mass transformation experiment. J. Meteorol. Soc. Jpn., 54, 382–398, https://doi.org/10.2151/jmsj1965.54.6_382, 1976.

Leith, C. E.: Theoretical skill of Monte Carlo forecasts. Mon. Wea. Rev., 102, 409–418, 1974.

Lin, Y.-L., Farley, R. D., and Orville, H. D.: Bulk parameterization of the snow field in a cloud model. J. Appl. Meteorol. Clim., 22, 1065–1092, 1983.

Louis, J. F., Tiedtke, M., and Geleyn, J. F.: A short history of the operational PBL parameterization at ECMWF, in: Proceedings of Workshop on Planetary Boundary Layer Parameterization, 25– 27 November 1981, Shinfield Park, Reading, UK, 59–79, 1982.

Lorenz, E.N.: The predictability of a flow which possesses many scales of motion. Tellus, 21, 289–307. https://doi.org/10.3402/tellusa.v21i3.10086, 1969.

Lorenz, E.N.: Atmospheric predictability as revealed by naturally occurring analogues. J. Atmos. Sci., 26, 636–646, 1969.

Murphy, J. M.: The impact of ensemble forecasts on predictability. Quart. J. Roy. Meteor. Soc., 114, 463–493, 1988.

Murakami, M.: Numerical modeling of dynamical and microphysical evolution of an isolated convective cloud – the 19 July 1981 CCOPE cloud. J. Meteorol. Soc. Jpn., 68, 107–128, 1990.

Murakami, M., Clark, T. L., and Hall, W. D.: Numerical simulations of convective snow clouds over the Sea of Japan: Two dimensional simulation of mixed layer development and convective snow cloud formation. J. Meteorol. Soc. Jpn. 72, 43–62, 1994.

Melhauser, C., and Zhang, F.: Practical and intrinsic predictability of severe and convective weather at the mesoscales. J. Atmos. Sci., 69, 3350–3371, doi:10.1175/JAS-D-11-0315.1, 2012.

Nhu, D. H., Anh, N. X., Phong, N. B., Quang, N. D., and Hiep, V. N.: The role of orographic effects on occurrence of the heavy rainfall event over central Viet Nam in November 1999. Journal of Marine Science and Technology. V. 17, No. 4B(2017), 31-36, 2017.

Nielsen, E.R. and Schumacher, R.S.: Using convection-allowing ensembles to understand the predictability of an extreme rainfall event. Monthly Weather Review, 144, 3651–3676, 2016.

750 Segami, A., Kurihara, K., Nakamura, H., Ueno, M., Takano, I., and Tatsumi, Y.:
751   Operational mesoscale weather prediction with Japan Spectral Model. J. Meteorol.
752   Soc. Jpn., 67, 907–924, https://doi.org/10.2151/jmsj1965.67.5_907, 1989.

753 Surcel, M., Zawadzki, I., and Yau, M. K.: On the filtering properties of ensemble
754   averaging for storm-scale precipitation forecasts. Mon. Wea. Rev., 142, 1093–1105,
755   doi:10.1175/ MWR-D-13-00134.1, 2014.

756 Son, B. M. and Tan, P. V.: Experiments of heavy rainfall prediction over South of Central
757   Viet Nam using MM5 (In VietNamese). Viet Nam Journal of Hydrometeorology.,
758   4(580), 9−18, 2009.

759 Toan, T. N., Thanh, C., Phuong, P. T., and Anh, T. V.: Assessing the predictability of WRF
760   model for heavy rain by cold air associated with the easterly wind at high-level patterns
761   over mid-central Viet Nam (In VietNamese). VNU Journal of Science: Earth and
762   Environmental Sciences. v. 34, n. 1S, dec. 2018. ISSN 2588-1094.
763   https://js.vnu.edu.vn/EES/article/view/4328, 2018.

764 Torn, R.D., Hakim, G.J.: Initial condition sensitivity of western Pacific
765   extratropical transitions determined using ensemble-based sensitivity analysis. Mon.
766   Weather Rev. 137, 3388–3406. https://doi.org/10.1175/2009MWR2879.1, 2009.

767 Tsuboki, K. and Sakakibara, A.: Numerical Prediction of HighImpact Weather Systems:
768   The Textbook for the Seventeenth IHP Training Course in 2007, Hydrospheric
769   Atmospheric Research Center, Nagoya University, Nagoya, Japan, and UNESCO,
770   Paris, France, 273 pp., http://www.rain.hyarc.nagoya-u.ac.jp/~tsuboki/
771   cress_html/src_cress/CReSS2223_users_guide_eng.pdf (last access: 1 May 2019),
772   2007.

773 Tuoi Tre news: https://tuoitre.vn/mien-trung-tiep-tuc-mua-lon-14-nguoi-chet-va-mat-tich-
774   20181212201907413.htm (last ac-cess: 5 June 2024), 2018

775 Wang, C.-C.*, Kuo, H.-C., Yeh, T.-C., Chung, C.-H., Chen, Y.-H., Huang, S.-Y.,

776   Wang, Y.-W., and Liu, C.-H.: High-resolution quantitative precipitation forecasts and

777   simulations by the Cloud-Resolving Storm Simulator (CReSS) for Typhoon Morakot

778   (2009). J.Hydrol., 506, 26-41, http://dx.doi.org/10.1016/j.jhydrol.2013.02.018, 2013.

779 Wang. C.-C.*, Lin, B.-X., Chen, C.-T., and Lo, S.-H.: Quantifying the effects of long-term

780   climate change on tropical cyclone rainfall using cloud-resolving models:

781   Examples of two landfall typhoons in Taiwan. J. Climate, 2015.

782 Wang, C.-C.: On the calculation and correction of equitable threat score for model

783   quantitative precipitation forecasts for small verification areas: The example of

784   Taiwan. Wea. Forecasting, 29, 788–798, doi:10.1175/WAF-D-13-00087.1, 2014.

785 Wang, C.-C., Huang, S.-Y., Chen, S.-H., Chang, C.-S., and Tsuboki, K.: Cloud resolving

786   typhoon rainfall ensemble forecasts for Taiwan with large domain and

787   extended range through time-lagged approach. Wea. Forecasting, 31,151–172,

788   doi:10.1175/WAF-D-15-0045.1, 2016.

789 Wang, C.-C., Li, M.-S., Chang, C.-S., Chuang, P.-Y., Chen, S.-H., and Tsuboki, K.:

790   Ensemble-based sensitivity analysis and predictability of an extreme rainfall event

791   over northern Taiwan in the Mei-yu season: The 2 June 2017 case. Atmos. Res., 259,

792   105684, https://doi.org/10.1016/j.atmosres.2021.105684, 2021.

793 Wang, C.-C., Tsai, C.-H., Jou, B. J.-D., and David, S. J.: Time-Lagged Ensemble

794   Quantitative Precipitation Forecasts for Three Landfalling Typhoons in the Philippines

795   Using the CReSS Model, Part I: Description and Verification against Rain-Gauge

796   Observations. Atmosphere, 13, 1193, https://doi.org/10.3390/atmos13081193, 2022.

797 Wang, C.-C., and Nguyen, D. V.: Investigation of an extreme rainfall event during 8–12

798   December 2018 over central Viet Nam – Part 1: Analysis and cloud-resolving

799   simulation. Nat. Hazards Earth Syst. Sci., 23, 771–788, https://doi.org/10.5194/nhess-

800   23-771-2023, 2023.

801 Wang, C.-C., Chen, S.-H., Chen, Y.-H., Kuo, H.-C., Ruppert, Jr., J. H., and Tsuboki, K.:
802   Cloud-resolving time-lagged rainfall ensemble forecasts for typhoons in Taiwan:
803   Examples of Saola (2012), Soulik (2013), and Soudelor (2015). Wea. Clim. Extremes,
804   40, 100555, https://doi.org/10.1016/j.wace.2023.100555, 2023.

805 Wilks, D. S.: Statistical Methods in the Atmospheric Sciences. Academic Press, 648 pp.,
806   ISBN 13: 978-0-12-751966-1, 10: 0-12- 751966-1, 2006.

807 Weyn, J.A., and Durran, D.R.: The scale dependence of initial-condition sensitivities in

808 simulations of convective systems over the southeastern United States. Q J R Meteorol
809   Soc.,145 (Suppl.1), 57–74, https://doi.org/10.1002/qj.3367, 2018.

810 Ying, Y., and Zhang, F.: Practical and intrinsic predictability of multi-scale weather and
811   convectively coupled equatorial waves during the active phase of an MJO. Journal of
812   the Atmospheric Sciences, 74(11), 3771–3785. https://doi.org/10.1175/JAS-D-17-
813   0157.1, 2017.

814